

# Limitations of dual-sgRNA CRISPR strategies for the treatment of CNS genetic disorders

Fábio Duarte<sup>1,2</sup> Gabriel Vachey<sup>1,2</sup>, Nicholas S. Caron<sup>3</sup>, Melanie Sipion<sup>1,2</sup>, Maria Rey<sup>1,2</sup>, Anselme L. Perrier<sup>4,5</sup>, Michael R. Hayden<sup>3</sup>, and Nicole Déglon<sup>1,2\*</sup>

<sup>1</sup>Lausanne University Hospital (CHUV) and University of Lausanne (UNIL), Department of Clinical Neurosciences (DNC), Laboratory of Cellular and Molecular Neurotherapies, Lausanne, Switzerland.

<sup>2</sup>Lausanne University Hospital (CHUV) and University of Lausanne (UNIL), Neuroscience Research Center (CRN), Laboratory of Cellular and Molecular Neurotherapies (LCMN), Lausanne, Switzerland.

<sup>3</sup>Centre for Molecular Medicine and Therapeutics, BC Children's Hospital and Research Institute, University of British Columbia, Vancouver, Canada. <sup>4</sup>Université Paris-Saclay, CEA, CNRS, Laboratoire des Maladies Neurodégénératives: mécanismes, thérapies, imagerie, Fontenay-aux-Roses, France.

<sup>5</sup>Université Paris-Saclay, CEA, Molecular Imaging Research Center, Fontenay-aux-Roses, France.

Short title : CNS gene editing limitations

Keywords: Huntington's disease, haplotypes, SNP, allele-selective, gene editing.

\*Corresponding author:

Nicole Déglon

Lausanne University Hospital (CHUV)

Laboratory of Cellular and Molecular Neurotherapies

Pavillon 3, Avenue de Beaumont

1011 Lausanne

Switzerland

Phone : +41 21 314 21 20

E-mail : [nicole.deglon@chuv.ch](mailto:nicole.deglon@chuv.ch)

## ABSTRACT

Huntington's disease (HD) is a fatal neurodegenerative disorder caused by a toxic gain-of-function CAG expansion in the first exon of the huntingtin (*HTT*) gene. The monogenic nature of HD makes mutant *HTT* inactivation a promising therapeutic strategy. Single nucleotide polymorphisms (SNPs) frequently associated with CAG expansion have been explored to selectively inactivate mutant *HTT* (*mHTT*) allele using the CRISPR/Cas9 system. One of such allele-selective approaches consists of excising a region flanking the first exon of *mHTT* by inducing simultaneous double-strand breaks at upstream and downstream positions of the *mHTT* exon 1. The removal of the first exon of *mHTT* deletes the CAG expansion and important transcription regulatory sites, leading to *mHTT* inactivation. However, the frequency of deletion events is yet to be quantified either *in vitro* or *in vivo*. Here, we developed accurate quantitative digital PCR-based assays to assess *HTT* exon 1 deletion *in vitro* and in fully humanized HU97/18 mice. Our results demonstrate that dual-sgRNA strategies are efficient and that 67% of *HTT* editing events are leading to exon 1 deletion in HEK293T cells. In contrast, these sgRNA actively cleaved *HTT* in HU97/18 mice, but most editing events do not lead to exon 1 deletion (10% exon 1 deletion). We also showed that the *in vivo* editing pattern is not affected by CAG expansion but may potentially be due to the presence of multiple copies of wt/*mHTT* genes HU97/18 mice as well as the slow kinetics of AAV-mediated CRISPR/Cas9 delivery.

## INTRODUCTION

Huntington's disease (HD) is a fatal neurodegenerative disorder caused by a CAG expansion in exon 1 of the huntingtin (*HTT*) gene.<sup>1</sup> The age of HD onset and disease progression inversely correlate with the CAG tract size, with full penetrance above 40 repeats.<sup>2</sup> Clinical manifestations arise between the ages of 35 and 50, with death occurring within the following 15 to 20 years. HD symptoms are strongly associated with the dysfunction and degeneration of spiny projecting neurons (SPNs) in the basal ganglia, which are an important relay in voluntary motor functions and various cognitive loops, including attention and memory.<sup>3,4</sup> The expanded CAG repeat encodes a longer polyglutamine (polyQ) domain present at the N-terminus of the HTT protein. This feature modifies the conformation of mutant HTT (mHTT) and induces aggregation.<sup>5</sup> Mutant HTT-mediated toxicity includes the dysregulation of several cellular pathways, such as axonal transport, transcription, translation, and mitochondrial and synaptic functions. The contribution of the expanded CAG repeats may extend beyond the encoded polyQ peptides, including toxicity mediated by the RNA containing the CUG expansion<sup>6,7</sup> and products derived from repeat associated non-AUG (RAN) translation.<sup>8</sup>

To date, there are no available therapies to modify disease progression. Given that HD is a gain-of-function disorder, strategies that target the disease-causing *HTT* (*mHTT*) gene and/or downstream products hold great therapeutic potential. Allele-selective strategies that target only the *mHTT* allele have been designed to preserve wtHTT functions.<sup>9,10</sup> Patients carrying the *mHTT* allele share common ancestors and, therefore, sets of single nucleotide polymorphisms (SNPs) are more strongly associated with the expanded *HTT* alleles.<sup>11-17</sup> The association of specific SNPs with the CAG expansion provides a unique opportunity to discriminate between the two *HTT* alleles. In parallel, the emergence of the CRISPR/Cas9 system has advanced the design of multiple approaches to permanently and selectively inactivate the *mHTT* allele as a therapeutic option.<sup>18-23</sup> Most of these studies have focused on the design of sgRNAs targeting SNPs that generate novel protospacer adjacent motifs (PAMs) in the mutant allele or delete PAMs from the wildtype allele (PAM-altering SNPs - PAS). This ensures that only the *mHTT* allele is cleaved by the Cas9 nuclease. One of the approaches involves the combination of two single guide RNAs (sgRNAs) to promote simultaneous cleavage at upstream and downstream sites of *mHTT* exon 1 to excise part of the promoter, the transcriptional and translation start sites as well as the first exon of the *mHTT* allele, leading to mutant HTT inactivation.<sup>18-20,22</sup> These studies have shown the feasibility of the approach *in vitro* in puromycin-enriched or clonal

lines of induced pluripotent cells from HD patients (HD-iPSCs). However, the efficiency of *HTT* exon 1 deletion *in vitro* in bulk cell populations and *in vivo* has not been reported.<sup>19</sup>

Given the ultimate goal of applying such dual-sgRNA strategies for the treatment of HD, it is critical to accurately assess their efficiency to determine and/or improve their therapeutic potential. Here, we developed quantitative digital PCR-based assays to accurately evaluate the efficiency of *HTT* exon 1 deletion *in vitro* and *in vivo* and present novel insights concerning the applicability of dual-sgRNA deletion approaches for the treatment of genetic disorders.

## MATERIALS AND METHODS

### Plasmid production

The sgHTT25A/G, sgHTT6T/C, sgHTT10C/G, sgHTT2G/A, and sgHTT4 were initially ordered as gene strands (IDT, Leuven, Belgium; Table S1) and cloned into the pENTR221 plasmid as previously described.<sup>24</sup> The lead candidates (sgHTT6T/C, sgHTT8P\_L, sgHTT8P\_S, sgHTT2G, and sgHTT4) were then cloned into optimized expression cassettes. We used the universal plasmid pMK-AttL1-NotI/BamHI-U6-BsaI-tracrRNAopt-BamHI/NcoI-U6-SapI-tracrRNAopt-NotI/NcoI/XbaI-7sk-BsmBI-tracrRNA-XbaI-AttL2 (Addgene, #190898) containing three sgRNA expression cassettes, to make possible a flexible cloning strategy for multiple sgRNAs. The U6-driven expression cassettes contain an optimized tracrRNA described by Dang et al.<sup>25</sup>, whereas the 7sk-driven expression cassette is associated with the original tracrRNA.<sup>24</sup> The spacer sequence of each sgRNA was then inserted into the universal entry plasmid with overhang-compatible annealed oligos after digestion of the plasmid with type IIS restriction enzymes (BsaI or SapI). The oligomers used to clone each sgRNA are described in Table S2. Briefly, the last 7sk-sgCas9 cassette was removed by XbaI digestion. We then generated the entry plasmids expressing two sgRNAs: the allele-selective sgRNA (sgHTT6T, sgHTT8P\_L, sgHTT8P\_S, or sgHTT2G) in first cassette and sgHTT4 in the second cassette (U6-sgHTT“X”-U6-sgHTT4). The entry plasmids expressing only one *HTT*-targeting sgRNA were subsequently produced by removing the first or second U6-driven expression cassettes by BamHI or NcoI digestion, respectively. The SIN and pAAV2ss plasmids were produced by transferring the sgRNA expression cassettes from the entry plasmids into a LV (SIN-cPPT-Gateway-PGK-mCherry-WPRE) or AAV destination vector (pAAV2ss-Gateway-WPRE-bGH), respectively.

For SIN plasmids expressing SpCas9, we used the SIN-cPPT-PGK-SpCas9-WPRE (Addgene, #87886)<sup>24</sup> for editing assessment in HEK293T cells. For HD-NPCs, we generated the SIN-cPPT-PGK-SpCas9-BPNLS-WPRE plasmid after replacing the SRAD and SV40-NLS of the previous construct with a glycine-serine linker<sup>26</sup> and a bipartite NLS (BPNLS).<sup>27,28</sup> For the AAV-based systems, we used pAAV2ss-EFS-SpCas9-synPolyA (a gift from Ryohei Yasuda; Addgene, #104588)<sup>29</sup>. In addition, we generated a plasmid expressing nuclear GFP (pAAV2ss-CBA-AcGFPnuc-WPRE-bGH) by transferring the AcGFPnuc coding sequence from the entry plasmid pENTR4-AttL1-AcGFPnuc-AttL2 to the pAAV2ss-CBA-Gateway-WPRE-bGH destination vector.

### **Human embryonic kidney 293T (HEK293T) cells**

HEK293T cells (mycoplasma-negative, ATCC, LGC Standards GmbH, Wessel, Germany) were cultured in DMEM-Glutamax supplemented with 10% FBS and 1% penicillin/streptomycin (Gibco, Life Technologies, Zug, Switzerland) at 37°C in an atmosphere containing 5% CO<sub>2</sub>. For routine culture, cells were passaged twice weekly after trypsin treatment for dissociation (Gibco, Life Technologies, Zug, Switzerland) and plated at a density of 2x10<sup>6</sup> cells/cm<sup>2</sup> in T175 flasks.

### **HD-derived neuronal precursor cells (HD-NPCs)**

Patient-derived neuronal progenitor cells (HD-NPCs) were generated from hPSC line GM03621 (Coriell) provided by Dr. Anselme Perrier (I-Stem, Evry, France). The differentiation and culture protocols have been previously described.<sup>30,31</sup> After amplification, HD-NPCs were banked in vials of 4x10<sup>6</sup> cells and stored in liquid nitrogen. For each experiment, cells were thawed and resuspended in N2B27 medium (1:1 ratio of DMEM-F12-Glutamax:Neurobasal, 1% N2 supplement, 2% B27 supplement, and 0.1% Gentamicin - Gibco, Life Technologies, Zug, Switzerland). Cells were centrifuged at 300 x g for 5 min to remove any traces of FBS and DMSO. The cell pellet was resuspended in 1 mL N2B27 medium and the cells counted using a hemocytometer. For cell expansion, approximately 1.5x10<sup>6</sup> and 10x10<sup>6</sup> of cells were plated in six-well plates or 10 cm dishes, respectively, in N2B27 medium supplemented with 10 ng/mL FGF (Bio-technie, Zug, Switzerland), 10 ng/mL EFG (Peprotech, Zug, Switzerland), and 20 ng/mL BDNF (Peprotech, Zug, Switzerland). Prior to plating, the wells/dishes were coated with 1:6 poly-L-ornithine (Sigma-Aldrich, Buchs, Switzerland) in H<sub>2</sub>O for 24 h and then with 2 µg/mL laminin (Sigma-Aldrich, Buchs, Switzerland) in H<sub>2</sub>O for 24 h. The medium was completely changed twice a week and the cells passed once a week.

### **Production of lentiviral vectors**

LVs were produced by the calcium phosphate-mediated transfection of HEK293T cells with a four-plasmid system.<sup>32</sup> Human immunodeficiency virus type 1 (HIV-1) vectors were pseudotyped with the vesicular stomatitis virus glycoprotein (VSV-G) envelope, concentrated by ultracentrifugation and resuspended in phosphate-buffered saline (PBS, Gibco, Life Technologies, Zug, Switzerland) supplemented with 1% bovine serum albumin (BSA, Sigma-Aldrich, Buchs, Switzerland). The viral

particle content of each batch was determined in a p24 antigen enzyme-linked immunosorbent assay (p24 ELISA, RETROtek, Kampenhout, Belgium). Viral stocks were stored at -80°C until use.

### **Production of adeno-associated vectors**

AAVs were produced in HEK293T cells by calcium phosphate-mediated transfection as previously reported.<sup>33</sup> The viral genome content (vg/mL) for each AAV was assessed by *TaqMan* qPCR using primers that recognize the inverted terminal repeats of the AAV2 viral genome (forward primer: 5'- GGAACCCCTAGTGATGGAGTT-3', reverse primer: 5'-CGGCCTCAGTGAGCGA-3', *TaqMan* probe: 5'- FAM-CACTCCCTCTCTGCGCGCTCG-TAMRA-3') and the KAPA probe fast qPCR universal kit (Sigma-Aldrich, Buchs, Switzerland). AAV vectors were stored at -80°C until use.

### **Transfection of HEK293T cells**

For the transfection experiments (Fig. 1C; Fig. 3, 5, S6), we plated  $5 \times 10^5$  cells per well in six-well plates the day before transfection. We mixed the plasmids in 0.25 M  $\text{CaCl}_2$  solution and the mixture was then added dropwise to HEPES saline buffer (Sigma-Aldrich, Buchs, Switzerland,  $\text{CaCl}_2$ -H<sub>2</sub>O:HEPES ratio 1:1). The mixture was incubated at room temperature for 5 min and added dropwise to the cells (10% of the culture volume). The medium was completely replaced 6 h after transfection. Transfected cells were lysed for DNA and/or RNA extraction at four days post-transfection.

To evaluate the efficiency and/or selectivity of the sgRNAs (Fig. 1C), HEK293T cells were transfected with 0.5  $\mu\text{g}$  SIN-cPPT-PGK-GFP-WPRE, 2  $\mu\text{g}$  SIN-cPPT-PGK-SpCas9-WPRE, and 2  $\mu\text{g}$  pENTR221 plasmids expressing sgRNA. The sgRNA expression was under the control of the H1 promoter for all sgRNAs, except sgHTT4, for which expression was driven by the U6 promoter. All sgRNAs had the backbone (tracrRNA) used in Merienne et al.<sup>24</sup> Cells solely transfected with the plasmid encoding SpCas9 and GFP were used as a negative control.

To assess *HTT* editing outcomes by agarose gel, digital PCR, and TIDE analyses (Fig. 3), HEK293T cells were transfected with 0.6  $\mu\text{g}$  pAAV2ss-CBA-GFP-WPRE-bGH, 1.1  $\mu\text{g}$  pAAV2ss-EFS-myc-SV40-spCas9-SV40-synPolyA, and 2.1  $\mu\text{g}$  pAAV2ss plasmids expressing sgHTT8P\_L and sgHTT4 (SpCas9:sgRNA molar ratio of 1:3). Cells solely transfected with pAAV2ss plasmids encoding SpCas9 and GFP were used as a negative control.

To compare *HTT* exon 1 deletion efficiency between transfected and transduced cells (Fig. 5, S6), HEK293T cells were transfected with 2 µg SIN-cPPT-PGK-Cas9-WPRE and 2 µg SIN plasmids expressing two sgRNAs plus mCherry. Expression of the sgRNAs and mCherry was driven by the U6 and PGK promoters, respectively. Cells solely transfected with SIN plasmids encoding SpCas9 and GFP were used as a negative control.

### **Generation of clonal HEK293T cell lines with *HTT* exon 1 deletion**

For the clonal analysis of HEK293T cells containing deletions of exon 1 from the *HTT* gene (Fig. S1),  $5 \times 10^6$  cells in 10 cm dishes were transfected 24 h after seeding with 30 µg of plasmid (15 µg SIN-cPPT-PGK-SpCas9-WPRE and 15 µg SIN-U6-sgHTT8P\_L-U6-sgHTT4-PGK-mCherry). Five days post-transfection, cells were dissociated with trypsin and serial dilutions plated in 96-well plates. The cell clones that grew at the highest dilution conditions were sequentially expanded in 48-well plates, 24-well plates, and six-well plates. Finally, we screened the clonal cell lines for the presence of exon 1 deletion from the *HTT* gene by PCR amplification.

### **Transduction of HEK293T cells**

For the transduction experiments in HEK293T cells (Fig. 1D, E; Fig. 5, S6), we plated  $5 \times 10^5$  cells per well in six-well plates the day before transduction. The cells were transduced with 200 ng LV (100 ng SIN-cPPT-PGK-Cas9-WPRE and 100 ng LV expressing the sgRNAs plus mCherry reporter) diluted in DMEM medium added dropwise to the cells (5% of the culture volume). Cells transduced with LVs encoding SpCas9 and mCherry with no sgRNAs were used as a negative control. The medium was completely replaced 24 h after transduction. Transduced cells were then passed once a week and lysed for DNA and RNA extraction at three weeks post-transduction.

### **Transduction of HD-NPCs**

For the transduction experiments in HD-NPCs (Fig. 2, S2), we plated  $8 \times 10^5$  cells per well in six-well plates the day before transduction. The cells were transduced with LV diluted in N2B27 medium added dropwise to the cells (5% of the culture volume). The medium was completely replaced 24 h after transduction. The transduced cells were then passed once a week and lysed for DNA and RNA extraction at two weeks post-transduction.

To evaluate the efficiency of HTT exon 1 deletion (Fig. 2), cells were transduced with 200 ng LV expressing SpCas9-BPNLS and 200 ng LV expressing HTT6/HTT4 or HTT8P/HTT4. To assess the individual editing efficiency of each sgRNA (Fig. S2), cells were transduced with 200 ng LV expressing SpCas9-BPNLS and 200 ng LV expressing each sgRNA. Cells transduced with LVs encoding SpCas9 and mCherry with no sgRNAs were used as a negative control.

## Animals

Transgenic mice expressing the full-length human wildtype and mutant *HTT* gene (HU97/18 - BACHD<sup>+</sup>; YAC18<sup>++</sup>; Hhd<sup>-/-</sup>) or only the full-length wildtype *HTT* gene (HU18/18 - YAC18<sup>++</sup>; Hhd<sup>-/-</sup>) were kindly provided by Prof. Hayden (Vancouver, Canada).<sup>34</sup> Adult male and female transgenic mice (9-10 weeks old) were used for the *in vivo* experiments. Mice were housed in a specific pathogen-free (SPF) facility with GM500 IVC cages (Techniplast) or rat R.BTM.U x /R.ICV.6 cages (Innovive, Paris, France) containing corn cob bedding placed in simple face Innorack rat racks (cat# RS.5.8.40), with no more than five mice per cage. The animals were maintained in a controlled-temperature room (22 ± 1°C), under a 14-hour light/10-hour dark cycle. The following enrichments were provided: two pieces of wipes, one cardboard tunnel, and one cardboard or polysulfide house with two entrances/exits. Food (SAFE® 150, Safe, Rosenberg, Germany) and water were provided *ad libitum*. All experimental procedures were performed in strict accordance with Swiss regulations concerning the care and use of laboratory animals (veterinary authorization 3682).

## Stereotaxic Injections

Anesthesia and surgical procedures were performed as previously described.<sup>24</sup> The mice striata were bilaterally injected with 4 µL AAV2/rh.10 (1.05x10<sup>10</sup> vg) per hemisphere at a rate of 0.5 µL/min at the coordinates +0.8 ; ±1.9 ; -3.3 (+0.8 mm rostral to Bregma; ±1.9 mm lateral to midline; and 3.3 mm ventral from the skull surface, with the tooth bar set at -3.3 mm). The needles were left in place for 5 min after injection and then slowly removed. During surgery, body temperature was controlled with a warming blanket (CMA 450 Temperature Controller, Phymep, Paris, France) and the eyes were protected with 0.2% Viscotears liquid gel (Novartis, Basel, Switzerland). Post-surgery analgesic treatment (acetaminophen, Dafalgan Upsa 1000 mg/750 mL) was administered in the drinking water for 72 h.

## **DNA, RNA, and protein extraction**

For *in vitro* experiments, genomic DNA and RNA were extracted using Trizol Reagent (Life Technologies, Zug, Switzerland) according to the manufacturer's instructions. Briefly, the culture medium was removed and the cells were washed three times with PBS (Gibco, Life Technologies, Zug, Switzerland). The cells were then lysed directly in the well with 1 mL Trizol. The gDNA was precipitated and purified in accordance with the protocol provided by the supplier. The final DNA pellet was then resuspended in nuclease-free water (Gibco, Life Technologies, Zug, Switzerland) by passive homogenization in increasing volumes of water for 24 to 72 h at room temperature. For the experiments including RNA analysis, RNA was precipitated from the aqueous phase and purified in accordance with the protocol supplied by the supplier. The final RNA pellet was then resuspended in nuclease-free water (Gibco, Life Technologies, Zug, Switzerland) by passive homogenization followed by vortexing. Finally, both gDNA and RNA concentrations were determined using a Nanodrop spectrophotometer (Thermo Fisher Scientific, Reinach, Switzerland). The gDNA and RNA were maintained at  $-20^{\circ}\text{C}$  and  $-80^{\circ}\text{C}$  for long-term storage, respectively. In addition, protein was extracted from wildtype and clonal HEK293T cell lines in RIPA buffer (R0278, Sigma) supplemented with a 1/200 dilution of protease inhibitor cocktail (P8340, Sigma-Aldrich, Buchs, Switzerland) and  $5\ \mu\text{M}$  Z-VAD-FMK (HY-16658B, Chemie Brunschwig, Basel, Switzerland), hereafter referred to as RIPA<sup>+</sup> buffer. Briefly, approximately  $1 \times 10^6$  cells were washed in PBS and  $50\ \mu\text{l}$  of RIPA<sup>+</sup> buffer was added to the cell pellet. The pellet was homogenized with a pellet mixer (VWR, Dietikon, Switzerland) and left on ice for 30 min. The protein extract was then centrifuged at  $18,000 \times g$  for 15 min at  $4^{\circ}\text{C}$  and the supernatant containing solubilized proteins collected into a new tube and stored at  $-80^{\circ}\text{C}$ .

For *in vivo* experiments, mice were euthanized by isoflurane overdose and the brains collected and cut into 1 mm-thick coronal slices. We collected 4 to 5 punch specimens/animal ( $\sim 1.5\ \text{mm}^3$  each) from the GFP-positive striatal area. Genomic DNA was extracted from each individual punch specimen using the AllPrep DNA/RNA/miRNA Universal Kit (Qiagen, Hombrechtikon, Switzerland) according to the manufacturer's recommendations. The gDNA was stored at  $-20^{\circ}\text{C}$ .

## **PCR and TIDE analysis**

The editing efficiency of the sgRNAs targeting *HTT* and SpCas9 were assessed by tracking of indels by decomposition (TIDE) analysis<sup>35</sup> on Sanger sequencing chromatograms of amplified DNA. The indel size range was set to 10 to 15 and the size of the decomposition window was adapted for reads of low quality or those containing repetitive sequences. The significance cutoff was set to 0.05 (<https://tide.nki.nl/>). Nucleic acid amplification was performed on 100 ng gDNA (extracted by Trizol) or 10 ng gDNA (extracted using the AllPrep DNA/RNA/miRNA Universal Kit) with the KAPA HiFi Hotstart kit (KAPA Biosystems, Labgene) according to the manufacturer's recommendations. The *HTT* gene was amplified using two sets of PCR primers. Set 1 amplifies a region of 2800 bp containing all sgRNA target sites, except the sgHTT25 target site, whereas primer set 2 amplifies a region of 2040 bp containing all sgRNA target sites, except the sgHTT4 target site (Fig. 1B). The PCR reaction with primer set 1 consisted of the primers 5'-CTCCAAGAAGTGGGAAC-3' (fwd1) and 5'-ACCACCGTGATCATGAACTAAA-3' (rev1), with a melting temperature of 55°C and an extension time of 90 s. The PCR reaction with primer set 2 consisted of the primers 5'-TCGAACTCCTGACCTCTGGT-3' (fwd2) and 5'-CTGCTGGAAGGACTTGAGGG-3' (rev2), with a melting temperature of 65°C and an extension time of 60 s. The primers used to generate the Sanger sequencing chromatograms for each sgRNA target site are illustrated in Figure 1B and described in Table S3.

### **Measurement of *HTT* exon 1 deletion**

For the semiquantitative analysis of *HTT* exon 1 deletion on agarose gels, the *HTT* gene was amplified using primer set 1. We measured the optical density of the PCR bands on the agarose gel using Fiji software. The optical density of each band was then normalized against the length of the amplicon. Finally, for each sample, the length-normalized optical density of the exon1-deleted amplicon was divided by the sum of the length-normalized optical densities of the deleted plus non-deleted amplicons.

The quantification of *HTT* exon 1 deletion using promoter, intronic, and LoxP assays was performed by digital PCR in QIAcuity 24-well nanoplates with 8500 partitions (QIAcuity® digital PCR, Qiagen, Basel, Switzerland). The promoter assay is a Taqman-based assay to detect the amplification of the *HTT* promoter sequence using the primers 5'-CACTTCACACACAGCTTCGC-3' and 5'-TTCTGCCTCACACAGCAAGG-3', with the probe 5'-FAM-TACAGTCTCACCACGCCCCG-BHQ1-3'. The intronic assay is based on the EvaGreen signal of amplified amplicons by the primers 5'-

TCGCAGGATGCGAAGAGTTG-3' and 5'-GTAAAAAGAACCCCCGCCCT-3'. The LoxP assay is a Taqman-based assay to detect amplification of the LoxP sequence present in the *mHTT* transgene of HU97/18 mice using the primers 5'-GCGGGATCCATAACTTCGTA-3' and 5'-ACTCGAAGGCCTTCATCAGC-3', with the probe 5'-FAM-ATTAATCGAGGTCGACCGCC-BHQ1-3'. EvaGreen-intronic, FAM-promoter, and FAM-LoxP signals were normalized against VIC signals generated by amplification of the poly(rC)-binding protein 2 (*PCBP2*) gene with the primers 5'-TTGTGTCTCCAGTCTGCTTG-3' and 5'-AGGTGGTGGTGGTGGTA-3',<sup>36</sup> with the probe 5'-VIC-CCCTCTCCTGGCTCTAAATGTTGTGT-BHQ1-3'. Two different reactions were set up according to the manufacturer's instructions in a 12  $\mu$ L volume. The reaction amplifying the *HTT* intronic region contained 4  $\mu$ L 3x QIAcuity EvaGreen PCR master mix (Qiagen, Basel, Switzerland), 0.4  $\mu$ M of each primer, and 3 units EcoRI-HF restriction enzyme. The second reaction, which simultaneously amplified the promoter or LoxP sequence and the *PCBP2* gene, contained 3  $\mu$ L 4x QIAcuity Probe PCR master mix (Qiagen, Basel, Switzerland), 0.8  $\mu$ M of each primer, 0.4  $\mu$ M of each probe, and 3 units EcoRI-HF restriction enzyme. Loaded plates were incubated for 10 min at RT for EcoRI-HF digestion, followed by DNA amplification: initial denaturation at 95°C for 2 min, 40 amplification cycles at 95°C, 60°C, and 72°C for 15 s each, and a final step at 40°C for 5 min. Finally, data analysis was performed using QIAcuity Software Suite 2.0.20 (Qiagen, Basel, Switzerland).

### **RNA expression analysis**

RNA (1000 ng) extracted using Trizol Reagent (Life Technologies, Zug, Switzerland) was first treated with RNase-free DNase (RQ1, Promega, Dubendorf, Switzerland), according to the manufacturer's protocol, to remove any traces of genomic DNA and diluted to 20 ng/ $\mu$ L. The cDNA was generated from 200 ng DNase-treated RNA using Superscript II (Thermo Fisher, Reinach, Switzerland) according to the manufacturer's guidelines. Two sets of primers were used to evaluate HTT mRNA expression. One set was comprised of the primers 5'-AGTGATTGTTGCTATGGAGCGG-3' and 5'-GCTGCTGGTTGGACAGAACTC-3' (targeting HTT exons 64 and 65, respectively).<sup>37</sup> The other set consisted of the primers 5'-CTGCACCGACCAAAGAAAGAAC-3' and 5'-CATAGCGATGCCAGAAAGTTTC-3' (targeting the HTT exon1/2 junction and exon 3, respectively).<sup>37</sup> We also amplified the peptidylprolyl isomerase B (*PPIB*) gene using the primers 5'-TTCCATCGTGTAATCAAGGACTTC-3' (targeting PPIB exon 3) and 5'-

GCTCACCGTAGATGCTCTTTC-3' (targeting PPIB exon 4) as a reference gene for the quantification.<sup>38</sup> Real-time quantitative PCR (RT-qPCR) was used to assess HTT expression in the clonal cell lines (Fig. S1C) with the KAPA SYBR Fast qPCR master mix (Sigma-Aldrich, Buchs, Switzerland) according to the manufacturer's protocol, using a Rotor gene device (Qiagen, Basel, Switzerland) and the following cycle parameters: 95°C for 180 s and then 40 cycles of 95°C for 3 s and 60°C for 10 s. Digital PCR in QIAcuity 24-well nanoplates with 8500 partitions (QIAcuity® digital PCR, Qiagen, Basel, Switzerland) was used to evaluate the impact of indels (Fig. 1E) on HTT expression in transduced HEK293T cells. Each reaction was set up according to the manufacturer's instructions in a 12- $\mu$ L volume containing 4  $\mu$ L 3x QIAcuity EvaGreen PCR master mix (Qiagen, Basel, Switzerland), 0.4  $\mu$ M *HTT* or *PPIB* forward and reverse primers, and 40 ng cDNA. Loaded plates were then subjected to the following temperature cycling: initial denaturation at 95°C for 2 min, 40 amplification cycles at 95°C, 60°C, and 72°C for 15 s each, and a final step at 40°C for 5 min. Finally, data analysis was performed using QIAcuity Software Suite 2.0.20 (Qiagen, Basel, Switzerland).

### **Virtual western blot**

Protein concentrations were assessed using a BCA kit (Thermo Fisher Scientific, Reinach, Switzerland) according to the recommended procedure. After dilution in 0.1X SB (ProteinSimple, Bio-Techne), 0.6  $\mu$ g of total protein extract was size-separated using the Jess capillary-based immunoassay system. Samples were processed according to the manufacturer's instructions using the 66-440 kDa separation module (SM-W008). The primary anti-huntingtin antibody clone 1HU-4C8 (MAB2166, Zug, Switzerland) (diluted 1/750) and the anti-vinculin antibody clone 3M13 (ZRB1089, Merck, Nottingham, UK) (diluted 1/50) were used to target the HTT and vinculin proteins, respectively. Huntingtin and vinculin were then detected by chemiluminescence with an anti-rabbit-HRP conjugate (043-026, ProteinSimple, Bio-Techne AG, Zug Switzerland) diluted 1/20 in the ready-to-use anti-mouse-HRP conjugate (DM-002, ProteinSimple, Bio-Techne AG, Zug, Switzerland). Compass software (version 6.1) was used for the analysis. Peaks were determined using the Gaussian fit method and the HTT and vinculin signals were used to calculate the HTT/vinculin ratios.

### **Statistical methods**

For the statistical analyses, we tested the hypotheses of normally distributed data to determine the most appropriate statistical test. Post-hoc analyses were performed using GraphPad Prism 9.1.0 software. ANOVA was used for comparisons of more than two groups and *t*-tests were used for comparisons between two groups. No specific method was used for sample randomization, sample-size estimation, or data inclusion/exclusion. All results are presented as the mean  $\pm$  SD.

## RESULTS

### Design and *in vitro* validation of allele-selective sgRNAs

We identified frequently occurring SNPs located 2 kb upstream and 1.3 kb downstream of the *HTT* transcription start site (GRCh38, chr4:3072744-3076049) to selectively excise *mHTT* exon 1 containing the expanded CAG tract and therefore inactivate mHTT expression. According to phase 3 of the 1000 genomes project, this region contains 6 SNPs located upstream of the CAG repeat with a minor allele frequency (MAF) in the general population above 10% (Table 1). These variants are also amongst the most common SNPs associated with mutant *HTT* alleles in this region.<sup>20,22</sup> In particular, Shin et al. estimated that the variant rs2857935 is heterozygous in 27.6% of HD patients, making it one of the most promising targets for the development of allele-selective therapeutic strategies based on *mHTT* exon 1 deletion.<sup>22</sup> This variant is also a SpCas9 PAS, meaning that it eliminates the PAM on the *wtHTT* allele and prevents its cleavage. We designed two PAM-based selective sgRNAs that target this PAS (sgHTT8P\_L and sgHTT8P\_S) that differ in the length of the protospacer sequence (22 nt and 17 nt, respectively) (Table 1). For the other variants, the sgRNAs were designed to target the SNP close to the seed region of the sgRNA sequence (sgHTT25, sgHTT6, sgHTT10, and sgHTT2), as mismatches in this region have been shown to highly affect DNA binding and SpCas9 activity.<sup>39-42</sup> We did not design a sgRNA targeting the SNP rs9996199 because it was previously shown to induce poor on-target cleavage.<sup>19</sup> As the *mHTT* allele should be simultaneously cleaved upstream and downstream of the CAG expansion to promote *mHTT* exon 1 deletion, we designed a sgRNA that targets a sequence in the first intron conserved between the *wtHTT* and *mHTT* alleles (sgHTT4) (Table 1), of which the cleavage is expected to be well tolerated, with a minor or no impact on *HTT* expression.

We first assessed the efficiency and selectivity of each individual sgRNA in transfected HEK293T cells. Although SpCas9 activity is aborted by PAS,<sup>18-23</sup> sgRNAs targeting SNPs in the seed region still have the potential to induce indels in the non-targeted allele (i.e. *wtHTT*). HEK293T cells are homozygous for all of the identified SNPs (Table 1). Thus, we designed sgRNAs that harbor the respective mismatch sequence at the SNP (hereafter called mismatch sgRNAs) to assess selectivity by simulating the SNP of the non-targeted allele (Fig. 1A, B). The gene editing efficiency of each individual sgRNA was determined by tracking indels by decomposition (TIDE) in HEK293T cells transfected with three plasmids encoding SpCas9, sgRNA, and GFP (Fig. 1C). Cells transfected with only the plasmids encoding SpCas9 and GFP were used as a negative control. Among the sgRNAs

targeting SNPs upstream of exon 1, sgHTT25A generated low levels of indels, whereas sgHTT6T, sgHTT10G, and sgHTT2G induced indels in more than 10% of *HTT* alleles (Fig. 1C). All of these sgRNAs generated significantly more indels than the respective sgRNAs containing the mismatch sequence in the seed region, with the sgHTT6T targeting SNP rs28431418 showing the highest selectivity. In addition, PAM-based sgHTT8P\_L and sgHTT8P\_S targeting the PAS rs2857935 also generated high levels of indels in the *HTT* gene ( $16.5 \pm 0.9\%$  and  $19.6 \pm 0.8\%$ , respectively). Finally, the non-allele-selective sgHTT4 located in intron 1 showed relatively high editing efficiency ( $13.8 \pm 1.0\%$ ) (Fig. 1C).

We then evaluated the impact of the most promising sgRNA candidates on *HTT* mRNA expression. To ensure a high level of editing by each sgRNA, we modified the sgRNA backbone (tracrRNA) to that described by Dang et al.,<sup>25</sup> which was shown to promote higher levels of sgRNA expression and higher editing efficiency. In addition, we used lentiviral vectors (LVs) to maximize delivery of the CRISPR system into HEK293T cells. Three weeks post-transduction, all sgRNAs showed higher *HTT* editing (between 70 and 91%) (Fig. 1D) than those delivered by transfection. In terms of the impact on *HTT* mRNA expression, sgHTT2G was the only sgRNA that induced a decrease in transcription relative to the control ( $p < 0.0001$ ) (Fig. 1E). The sgHTT2G targets a promoter region close to the transcription start sites and indels at this position (rs13102260) may disrupt critical transcription factor binding sites and/or destabilize the nascent *HTT* mRNA. Importantly, despite high levels of gene editing ( $91.2 \pm 3.4\%$ ) (Fig. 1D), the intronic non-allele-selective sgHTT4 did not show any significant impact on *HTT* transcription relative to the control ( $p = 0.9986$ ) (Fig. 1E).

In conclusion, sgRNAs targeting SNPs in the *HTT* promoter displayed high editing efficiencies. As expected, the PAS-targeting sgHTT8P\_S and sgHTT8P\_L selectively cleaved the mutant *HTT* due to PAM incompatibility in the *wtHTT* allele<sup>19</sup> and sgHTT6T showed the highest selectivity for the targeted *mHTT* allele. Finally, sgRNA targeting intron 1 of *wtHTT* and *mHTT* (sgHTT4) has no major impact on *HTT* transcription.

### **Combining allele-selective sgRNAs with sgHTT4 to excise *mHTT* exon 1**

We then tested our dual-sgRNA strategy to inactivate the mutant *HTT* allele, by combining the sgRNAs targeting the promoter and intron 1 (Fig. 2). To detect the occurrence of *HTT* deletion events, we designed a PCR-based amplification assay using the primer set 1 (fwd1 and rev1; Fig. 2). Full-length

amplicons of approximately 2800 bp should result from the amplification of *HTT* loci, whereas the combined expression of sgHTT6T/sgHTT4 (hereafter named HTT6/4) and sgHTT8P\_L/sgHTT4 (hereafter named HTT8P/4) would result in the deletion of the corresponding genomic DNA and in the amplification of smaller amplicons of 974 bp and 1053 bp. We confirmed, as previously reported,<sup>19</sup> that these deletions are associated with a loss of HTT mRNA and protein expression, by analyzing *HTT*-edited HEK293T clones (Fig. S1). We then evaluated the dual-sgRNA strategy in a more relevant HD cellular model. We used neuronal precursor cells (HD-NPCs) generated from iPSCs derived from the patient fibroblast line GM03621 (Coriell Institute for medical research) carrying 18 CAGs in the *wtHTT* allele and 59 in the *mHTT* allele. These cells are heterozygous for rs2857935 (targeted by sgHTT8P\_L) and homozygous for rs28431418 (targeted by sgHTT6T) (Table 1). We co-transduced these HD-NPCs with LVs expressing SpCas9 and HTT6/4 or HTT8P/4 (Fig. 2). HTT8P/4 should exclusively inactivate the *mHTT*, whereas HTT6/4 should target both alleles (Fig. 2A). Two weeks post-transduction, we performed a semiquantitative analysis of the PCR products by agarose gel electrophoresis. Deletion events in *HTT* gene reached  $33.9 \pm 1.2\%$  for HTT6/4 and  $21.0 \pm 3.3\%$  for HTT8P/4 (Fig. 2B, C). The lower deletion efficiency of HTT8P/4 was anticipated, as only the *mHTT* alleles should be excised. Even though the intended outcome of dual-sgRNA strategies is the excision of genomic regions, other editing events such as inversions, integrations and/or indels are also likely to take place in non-truncated *HTT* alleles<sup>43,44</sup>. To evaluate the presence of other edits in the *HTT* gene, we measured the frequency of indels by isolating and sequencing the *wtHTT* and *mHTT* full-length amplicons. The sgHTT4 showed high editing efficiency and sgHTT6T induced indels in both the *wtHTT* and *mHTT* alleles ( $33.9 \pm 2.86\%$  and  $38.3 \pm 6.2\%$ ). By contrast, indels at the sgHTT8P\_L site were limited and mainly detected in the *mHTT* alleles ( $2.6 \pm 0.5\%$  and  $9.8 \pm 1.6\%$ ) (Fig. 2D). The 3 to 5-fold lower editing efficiency of sgHTT8P\_L relative to sgHTT6T and sgHTT4 was not expected, as all sgRNAs showed comparable editing efficiency in transduced HEK293T cells (Fig. 1D). We confirmed this phenomenon in a second experiment in HD-NPCs transduced with LVs expressing each sgRNA individually (Fig. S2). The lower editing efficiency in HD-NPCs for sgHTT8P\_L and sgHTT8P\_S may be related to specific cell type-dependent genomic architecture and/or DNA repair mechanisms at this locus. These results highlight the need for caution when extrapolating sgRNA editing efficiencies to different cell types. In summary, we confirmed that excision of a region flanking exon 1 induces HTT inactivation with corresponding reduction of HTT mRNA and protein levels.<sup>19,20,22,23,45</sup> In addition, we showed that dual-sgRNA

strategies induce complex cell type-dependent editing patterns that involve the expected deletions but also cleavage at each target sites without deletion.

### **The major gene editing outcome of dual-sgRNA strategies in transfected HEK293T cells is the excision of genomic fragments**

Agarose gel analysis has been widely used to detect genomic deletion/insertions,<sup>46,47</sup> but it introduces bias due to the amplification of fragments of different sizes. To overcome this limitation, we developed two digital PCR-based (dPCR) assays (Fig. 3A). The promoter assay relies on the amplification of a *HTT* promoter sequence located downstream of the sgHTT8P\_L target site, whereas the intronic assay amplifies an *HTT* intronic sequence upstream of the sgHTT4 target site. The quantification of *HTT* exon 1 deletion events is thus based on the loss of promoter and/or intronic amplification signals after normalization against reference signals generated by the amplification of a conserved sequence in the poly(rC)-binding protein 2 (*PCBP2*) gene<sup>36</sup> (Fig. 3A). To validate the assays, we mixed genomic DNA from fully humanized HU97/18 transgenic mice (carrying human *HTT* transgenes)<sup>34</sup> with DNA from wildtype mice (mouse *Hdh* not amplified in either assay) in decreasing proportions to simulate the progressive loss of human *HTT* exon 1 (Fig. S3). Both assays accurately predicted the relative loss of human *HTT* exon 1 relative to the parental genomic sample from HU97/18 mice (Fig. S3). We then co-transfected HEK293T cells with plasmids expressing SpCas9<sup>AAV</sup>, sgHTT8P\_L/sGHTT4, and GFP and compared the frequency of *HTT* truncation events using both agarose gel analysis and digital PCR assays. Semiquantitative analysis of the agarose gel indicated that  $75.2 \pm 0.9\%$  of all *HTT* alleles were depleted of exon 1 (Fig. 3B, C), whereas both promoter and intronic digital PCR assays indicated that exon 1 was deleted from only  $29.9 \pm 2.4\%$  and  $28.6 \pm 5.2\%$  of the *HTT* alleles, respectively (Fig. 3D). These results confirm that agarose gel analysis greatly overestimates the frequency of deletion events. As previously demonstrated in HD-NPCs (Fig. 2), dual-sgRNA strategies induced complex editing outcomes, including exon 1 deletions and indels. TIDE analysis indicated that  $16.9 \pm 1.7\%$  and  $20.3 \pm 2.2\%$  of the non-deleted *HTT* alleles contained indels at the sgHTT8P\_L and sgHTT4 target sites, respectively (Fig. 3E). The overall gene editing pattern in transfected HEK293T cells with HTT8P/HTT4 is illustrated in Figure 3F. As exon 1 was deleted from approximately 30% of the *HTT* alleles (Fig. 3D) and 20% of the remaining full-length *HTT* alleles contained indels in at least one of the sgRNA target sites (Fig. 3E), it can be assumed that approximately

56% of the *HTT* alleles were not edited. Focusing on the edited alleles, 67% of the editing events deleted the *HTT* exon 1, whereas 23% introduced indels at the sgRNA target sites (Fig. 3F).

In conclusion, we demonstrate that agarose gel analysis overestimates the frequency of genomic deletion events, and that *HTT* exon 1 deletion is the major editing outcome in HEK293T cells transfected with HTT8P/HTT4.

### Dual-sgRNA strategies favor indels over deletion events *in vivo*

We then evaluated the efficiency of *HTT* exon 1 deletion in HU97/18 transgenic mice.<sup>34</sup> This mouse model was generated by crossbreeding BACHD transgenic mice, which express full-length human *mHTT*,<sup>48</sup> with YAC18 transgenic mice, which express full-length human *wtHTT*,<sup>49</sup> on a *Hdh(-/-)* background. This cross recapitulates the genetics of human HD, including the common A/C haplotype combination.<sup>17</sup> As a first proof of principle, we selected the HTT6/HTT4 combination to induce deletion of the *HTT* exon 1, even though the *wtHTT* and *mHTT* transgenes are homozygous for the SNP rs28431418 targeted by sgHTT6T (Table 1). We co-injected the striatum of HU97/18 mice with AAV2/rh.10 vectors expressing SpCas9<sup>AAV</sup> and HTT6/HTT4 (Fig. 4). As a control, AAV2/rh.10 vectors expressing the sgRNAs and a nuclear GFP reporter were used. The animals were euthanized four weeks post-injection. Striatal punches were collected from the GFP-positive areas for DNA extraction. Quantification of the deletion events using the intronic assay indicated that exon 1 was deleted from only  $4.8 \pm 4.0\%$  of the *HTT* transgenes ( $p=0.017$ ) (Fig. 4C). We also analyzed the frequency of indels in the full-length *HTT* amplicons to exclude a low frequency of deletion events due to the lack of activity of one of the sgRNAs *in vivo*. TIDE analysis showed that sgHTT6T and sgHTT4 induced  $43.8 \pm 6.5\%$  and  $21.8 \pm 5.6\%$  indels in the non-truncated *HTT* alleles, respectively (Fig. 4D). These results demonstrate that both sgRNAs actively cleaved *HTT*, but most of the cleavage events did not result in the deletion of exon 1 (Fig. 4E). If we only consider *HTT* editing events, 90% of introduced indels at the sgRNA target sites, while only 10% resulted in the truncation of *HTT*. Such a low deletion:indel ratio of the *HTT* editing events could be due to the presence of an expanded CAG tract, lowering the editing efficiency. We tested this hypothesis by designing an additional digital PCR assay (LoxP assay) to specifically assess exon 1 deletion events in mutant *HTT* transgenes (Fig. S4A, B). The LoxP assay gave similar results, with only  $3.6 \pm 3.4\%$  of *mHTT* transgenes carrying deletions of exon 1 (Fig. S4C). We performed an additional experiment in HU18/18 mice carrying only *wtHTT* transgenes and

confirmed that the expanded CAG has no impact on *HTT* truncation efficiency (Fig. S5). Another potential explanation for the higher proportion of indels over deletion events in edited *HTT* transgenes could be unbalanced activity of the two sgRNAs (Fig. 4D; Fig. S5D). The sgHTT6T induced 2 to 2.7-fold more indels than sgHTT4 in both the HU97/18 and HU18/18 models. Imbalances in sgRNA activity could promote asynchronous cleavage of the *HTT* gene by the two sgRNAs, reducing the chances to truncate and inactivate *HTT* gene. Whether the lower levels of indels generated by sgHTT4 is due to decreased sgRNA activity or to more accurate repair of double-strand breaks at this locus is yet to be elucidated. In conclusion, these results indicate that most of the *HTT* editing events induced by the dual-sgRNA strategy in HU97/18 and HU18/18 mice do not correspond to the intended deletion of exon 1.

### **The dynamics of dual-sgRNA strategies influences gene editing outcomes**

While 67% of the editing events deleted the *HTT* exon 1 in transfected HEK293T cells (Fig. 3F), more than 90% of the editing events *in vivo* introduced indels at the sgRNA target sites (Fig. 4E; Fig. S5E). The contrasting deletion:indel ratios could be explained by the kinetics of the CRISPR/Cas9 system. Cell transfection promotes rapid and high CRISPR/Cas9 activity, whereas viral vector delivery into the mouse brain leads to a moderate incremental increase in CRISPR/Cas9 editing over time. The low CRISPR/Cas9 editing activity at the initial stages of viral transduction could promote the occurrence of more temporally sparse cleavage events, favoring the introduction of indels at one of the target sites before cleavage at the second site takes place. The shorter time window required for the CRISPR/Cas9 system to achieve maximal activity in transfected HEK293T cells would reduce the likelihood of non-simultaneous cleavage at the two target sites, favoring *HTT* exon 1 deletions over the introduction of indels. We tested this hypothesis by delivering the CRISPR systems expressing HTT6/HTT4 or HTT8P/HTT4 into HEK293T cells by transfection or lentiviral vector transduction (Fig. 5A). Genomic DNA was extracted four days post-transfection or two weeks post-transduction and the frequency of deletion and indel events were measured by digital PCR and TIDE analysis, respectively (Fig. S6). Digital PCR analysis showed frequencies of *HTT* exon 1 deletion ranging from 16 to 31% in cells treated with HTT8P/4 and HTT6/4, with no significant differences between transfection and transduction (Fig. S6A). By contrast, TIDE analysis showed that non-truncated *HTT* alleles in transduced cells contained at least four-fold more indels at the sgRNA target sites than in transfected cells (Fig. S6B). Overall, 41

to 45% and 85 to 91% of the *HTT* alleles carried deletions or indels in transfected and transduced cells, respectively (Fig. 5B; Fig. S6C). As highlighted in Figure 1, greater overall *HTT* editing efficiency in transduced cells was expected, given the higher competence of LVs to deliver the CRISPR system. While the deletion of exon 1 was detected in approximately 70% of the edited *HTT* alleles in transfected cells, only 17 to 31% of the edited *HTT* alleles were truncated in transduced cells (Fig. 5B). The lower deletion:indel ratio in transduced cells than in transfected cells supports the hypothesis that weak CRISPR/Cas9 activity at the initial phases of viral transduction favors the occurrence of single-cut over double-cut/deletion events. Overall, these results suggest that the frequency of deletion events induced by dual-sgRNA CRISPR systems may depend not only on balanced activity between the two sgRNAs, but also on the dynamics of the CRISPR activity.

## DISCUSSION

Given the wide-range of cellular functions associated with wtHTT, it is still unclear whether the loss of wtHTT activity would induce long-term deleterious effects.<sup>9</sup> One of the current approaches to specifically inactivate the *mHTT* allele consists of the selective excision of a region flanking *mHTT* exon 1 using dual-sgRNA strategies.<sup>18–20,22</sup> The feasibility of such approaches was demonstrated by PCR amplification, showing exon 1-deleted *mHTT* fragments in treated HD-iPSC lines after clonal or puromycin selection. In addition, Monteys et al. also detected *mHTT* exon 1 deletion in the striatum of treated BACHD mice.<sup>19</sup> However, none of these studies assessed the efficiency of *mHTT* exon 1 deletion *in vitro* or *in vivo*. In addition, similar dual-sgRNA strategies have also been proposed for other CNS disorders, but with no reports available concerning their efficiency.<sup>47</sup>

Here, we developed digital PCR-based assays to explore the efficiency and limitations of dual-sgRNA strategies aiming to delete *HTT* exon 1. Because the co-expression of two sgRNAs can induce complex editing outcomes, we combined digital PCR assays with TIDE analysis to assess *HTT* exon 1 deletion and assess the presence of indels in non-truncated *HTT* alleles to characterize the proportion of these gene editing events. We observed deletion events to be the major editing outcomes in transfected HEK293T cells (67-68%), but they were less frequent in transduced HEK293T cells (15-30%) and rare in the striatum of HU97/18 and HU18/18 mice (less than 10%). Recently, Simpson et al. highlighted the challenges of dual-sgRNA strategies to delete genomic sequences in the brain.<sup>43</sup> By combining two sgRNAs to eliminate the expanded CAG tract from the human *ATXN2* transgene in two SCA2 mouse models, the authors also observed that AAV fragment integration (22- 26%) and indels (22-30%) occurred much more frequently than CAG deletions (1-4%). In addition, another study attempting to delete exon 23 of the *DMD* gene *in vivo* reported that deletion events were almost absent in all analyzed organs, except the liver, where *DMD* exon 23 was deleted in 5% of the alleles.<sup>44</sup> Finally, a dual-sgRNA deletion strategy has been clinically tested for the treatment of Leber congenital amaurosis type 10 (LCA10) (EDIT-101 - NCT03872479). The injection of EDIT-101 was estimated to induce deletion/inversion events in 3 to 28% of the *CEP290* alleles of retinal photoreceptor cells of primates.<sup>50</sup> Even though low levels of deletion/inversion (10%) were estimated to be required to induce phenotypic improvement, the trial recently paused enrollment due to lack of efficacy, with only 3 of 14 patients showing clinical improvement. Whether these disappointing results are due to poor *CEP290*

gene correction in the photoreceptor cells of the patients is unknown. Overall, these results highlight the challenges of application of dual-sgRNA strategies aiming to delete genomic sequences *in vivo*.

In the *in vivo* experiments, we observed that sgHTT6T induced 2 to 2.7-fold more indels than sgHTT4 in both HU97/18 and HU18/18 mice. The lower deletion:indel ratio *in vivo* can be explained by asynchronous cleavage of the *HTT* gene as a consequence of an imbalance in the activity between the two sgRNAs. This hypothesis was previously postulated by Simpson et al., who also detected different frequencies of indels in the two sgRNA target sites.<sup>43</sup> The sgRNA activity depends on several factors, such as chromatin accessibility<sup>51</sup> and sgRNA secondary structure.<sup>52</sup> Thus, precisely tuning the activity of two sgRNAs could be very challenging. In addition, we showed that the activity of some sgRNA is cell type-specific. Equivalent loci-specific repair mechanisms and/or epigenetic states could also promote disparities in the indel frequencies induced by the two sgRNAs,<sup>51</sup> decreasing the chances of occurrence of simultaneous double-strand breaks. Finally, the low deletion:indel ratio observed *in vivo* may also be related to the existence of multiple transgene copies in HU97/18 and HU18/18 mice.<sup>23,33</sup> We have previously shown that HU97/18 carries 8 transgene copies (4 of *mHTT* and 4 of *wtHTT*), whereas HU18/18 carries 4 copies of *wtHTT*.<sup>33</sup> The higher number of sgRNA target sites would decrease the likelihood that spCas9 would simultaneously cut the copy of the transgene. It would be interesting to evaluate this strategy in models carrying a unique copy of the human *mHTT*. However, all the existing HD mouse models are either transgenic, or partial knock-in models lacking the human *HTT* promoter regulatory sequences. The development of more physiological relevant models such as knock-in mouse models carrying a single copy of the human *mHTT* and *wtHTT* genes along with regulatory sequences will be essential to further elucidate the impact of multiple transgenes in CRISPR/Cas9-based therapeutic strategies.

The differences observed between transfected and transduced HEK293T cells suggest that the delivery method strongly affects gene editing outcomes of dual-sgRNA strategies. We hypothesize that the gradual viral-mediated delivery of CRISPR promotes the occurrence of temporally sparse cleavage events at the initial stages of transduction, narrowing the probability of both sgRNAs simultaneously cleaving the *HTT* gene to delete exon 1. This interpretation is supported by the extremely low frequency of deletion events compared to indels observed *in vivo* after AAV-mediated delivery of the dual-sgRNA CRISPR system. To further reinforce this hypothesis, it would be informative to evaluate whether the frequency of deletion events can be improved in cells transfected with Cas9/gRNA ribonucleoprotein

complexes or light-activated systems, which would assure high and immediate activity of the CRISPR system. Nevertheless, while such approaches could potentially improve deletion outcomes *in vitro*, non-viral delivery strategies are still limiting to target the CNS *in vivo*.

Finally, the generation of genomic rearrangements including large chromosomal deletions, inversions, translocations or retrotransposon integration at CRISPR/Cas9 target sites bring safety issues, especially when therapeutic approaches are designed for *in vivo* applications.<sup>53</sup> Such events are likely to occur more frequently when using dual-sgRNA approaches due to increased incidence of DSBs. Recently, alternative allele-specific strategies have been proposed to specifically degrade the *mHTT* transcript by non-mediated mRNA decay using a single sgRNA.<sup>21,23</sup> In addition, the novel prime editing-based method PRIME-Del also holds a huge potential not only to improve deletion outcomes but also to decrease off-target events.<sup>54</sup> In the future, advantages and disadvantages of these approaches should be taken into account to develop the most efficient and safer allele-specific editing-based strategies for HD.

## CONCLUSIONS

We demonstrate that dual-sgRNA strategies to delete *HTT* exon 1 induce relatively frequent excision events *in vitro* but very rarely *in vivo*. Importantly, we present novel insights regarding the applicability of dual-sgRNA deletion approaches by demonstrating that CRISPR activity dynamics strongly influence the gene editing outcomes and frequency of intended deletion events.

## **ACKNOWLEDGMENTS**

We also thank Manfredo Quadroni, and Séverine Lorrain from the University of Lausanne (UNIL) Protein Analysis Facility for the Jess capillary western analyses.

## **AUTHOR CONTRIBUTIONS**

FD: conceptualization, investigation, methodology, formal analysis, validation, visualization, writing – original draft; GV: conceptualization, investigation, methodology, formal analysis, validation; NSC: methodology, funding acquisition; MS and MR: investigation, validation; ALP: resources, project administration; MRH: resources, project administration, funding acquisition; ND: conceptualization, project administration, resources, supervision, funding acquisition, visualization, writing – original draft; All authors: writing -review & editing.

## **CONFLICT OF INTERESTS**

All authors declare no conflict of interests.

## **FUNDING**

This work was partially supported by the Swiss National Science Foundation (FN 310030\_184761/1) and the European Union's Horizon 2020 research and innovation program under grant agreement No 31ER30\_179594 (TreatPolyQ).

## **DATA AVAILABILITY**

The most relevant plasmids are deposited at addgene ([https://www.addgene.org/Nicole\\_Deglon/](https://www.addgene.org/Nicole_Deglon/)).

## REFERENCES

1. MacDonald ME, Ambrose CM, Duyao MP, et al. A novel gene containing a trinucleotide repeat that is expanded and unstable on Huntington's disease chromosomes. *Cell*. 1993;72(6):971-983. doi:10.1016/0092-8674(93)90585-E
2. Andrew SE, Goldberg YP, Kremer B, et al. The relationship between trinucleotide (CAG) repeat length and clinical features of Huntington's disease. *Nat Genet* 1993;4(4):398-403. doi:10.1038/ng0893-398
3. Ross CA, Aylward EH, Wild EJ, et al. Huntington disease: natural history, biomarkers and prospects for therapeutics. *Nat Rev Neurol*. 2014;10(4):204-216. doi:10.1038/nrneurol.2014.24
4. Bates GP, Dorsey R, Gusella JF, et al. Huntington disease. *Nat Rev Dis Prim*. 2015;1(1):1-21. doi:10.1038/nrdp.2015.5
5. DiFiglia M, Sapp E, Chase KO, et al. Aggregation of huntingtin in neuronal intranuclear inclusions and dystrophic neurites in brain. *Science*. 1997;277(5334):1990-1993. doi:10.1126/SCIENCE.277.5334.1990/ASSET/7433F340-81EB-4536-932B-F1DD8E97A9B0/ASSETS/GRAPHIC/SE3975752005.JPEG
6. Chung DW, Rudnicki DD, Yu L, Margolis RL. A natural antisense transcript at the Huntington's disease repeat locus regulates HTT expression. *Hum Mol Genet*. 2011;20(17):3467-3477. doi:10.1093/HMG/DDR263
7. Nalavade R, Griesche N, Ryan DP, Hildebrand S, Krauß S. Mechanisms of RNA-induced toxicity in CAG repeat disorders. *Cell Death Dis*. 2013;4(8):e752-e752. doi:10.1038/cddis.2013.276
8. Bañez-Coronel M, Ayhan F, Tarabochia AD, et al. RAN Translation in Huntington Disease. *Neuron*. 2015;88(4):667-677. doi:10.1016/J.NEURON.2015.10.038
9. Kaemmerer WF, Grondin RC. The effects of huntingtin-lowering: what do we know so far? *Degener Neurol Neuromuscul Dis*. 2019;9:3-17. doi:10.2147/DNND.S163808
10. Rook ME, Southwell AL. Antisense Oligonucleotide Therapy: From Design to the Huntington Disease Clinic. *BioDrugs*. 2022;36(2):105-119. doi:10.1007/S40259-022-00519-9
11. Warby SC, Montpetit A, Hayden AR, et al. CAG Expansion in the Huntington Disease Gene Is Associated with a Specific and Targetable Predisposing Haplogroup. *Am J Hum Genet*. 2009;84(3):351-366. doi:10.1016/J.AJHG.2009.02.003

12. Warby SC, Visscher H, Collins JA, et al. HTT haplotypes contribute to differences in Huntington disease prevalence between Europe and East Asia. *Eur J Hum Genet.* 2011;19(5):561-566. doi:10.1038/ejhg.2010.229
13. Kay C, Collins JA, Caron NS, et al. A Comprehensive Haplotype-Targeting Strategy for Allele-Specific HTT Suppression in Huntington Disease. *Am J Hum Genet.* 2019;105(6):1112-1125. doi:10.1016/J.AJHG.2019.10.011
14. Chao MJ, Gillis T, Atwal RS, et al. Haplotype-based stratification of Huntington's disease. *Eur J Hum Genet.* 2017;25(11):1202-1209. doi:10.1038/ejhg.2017.125
15. Lee JM, Kim KH, Shin A, et al. Sequence-Level Analysis of the Major European Huntington Disease Haplotype. *Am J Hum Genet.* 2015;97(3):435-444. doi:10.1016/J.AJHG.2015.07.017
16. Lee JM, Gillis T, Mysore JS, et al. Common SNP-Based Haplotype Analysis of the 4p16.3 Huntington Disease Gene Region. *Am J Hum Genet.* 2012;90(3):434-444. doi:10.1016/J.AJHG.2012.01.005
17. Kay C, Collins JA, Skotte NH, et al. Huntingtin Haplotypes Provide Prioritized Target Panels for Allele-specific Silencing in Huntington Disease Patients of European Ancestry. *Mol Ther.* 2015;23(11):1759-1771. doi:10.1038/MT.2015.128
18. Shin JW, Kim KH, Chao MJ, et al. Permanent inactivation of Huntington's disease mutation by personalized allele-specific CRISPR/Cas9. *Hum Mol Genet.* 2016;25(20):4566-4576. doi:10.1093/HMG/DDW286
19. Monteys AM, Ebanks SA, Keiser MS, Davidson BL. CRISPR/Cas9 Editing of the Mutant Huntingtin Allele In Vitro and In Vivo. *Mol Ther.* 2017;25(1):12-23. doi:https://doi.org/10.1016/j.ymthe.2016.11.010
20. Fang L, Monteys AM, Dürr A, et al. Haplotyping SNPs for allele-specific gene editing of the expanded huntingtin allele using long-read sequencing. *Hum Genet Genomics Adv.* 2023;4(1):100146. doi:10.1016/j.xhgg.2022.100146
21. Shin JW, Hong EP, Park SS, et al. Allele-specific silencing of the gain-of-function mutation in Huntington's disease using CRISPR/Cas9. *JCI Insight.* 2022;7(19). doi:10.1172/JCI.INSIGHT.141042
22. Shin JW, Hong EP, Park SS, et al. PAM-altering SNP-based allele-specific CRISPR-Cas9 therapeutic strategies for Huntington's disease. *Mol Ther - Methods Clin Dev.* 2022;26:547-

561. doi:10.1016/J.OMTM.2022.08.005
23. Oikemus SR, Pfister EL, Sapp E, et al. Allele-Specific Knockdown of Mutant Huntingtin Protein via Editing at Coding Region Single Nucleotide Polymorphism Heterozygosities. *Hum Gene Ther.* 2022;33(1-2):25-36. doi:https://doi.org/10.1089/hum.2020.323
  24. Merienne N, Vachey G, de Longprez L, et al. The Self-Inactivating KamiCas9 System for the Editing of CNS Disease Genes. *Cell Rep.* 2017;20(12):2980-2991. doi:https://doi.org/10.1016/j.celrep.2017.08.075
  25. Dang Y, Jia G, Choi J, et al. Optimizing sgRNA structure to improve CRISPR-Cas9 knockout efficiency. *Genome Biol.* 2015;16(1):1-10. doi:https://doi.org/10.1186/s13059-015-0846-3
  26. Zhao P, Zhang Z, Lv X, et al. One-step homozygosity in precise gene editing by an improved CRISPR/Cas9 system. *Cell Res.* 2016;26(5):633-636. doi:10.1038/cr.2016.46
  27. Suzuki K, Tsunekawa Y, Hernandez-Benitez R, et al. In vivo genome editing via CRISPR/Cas9 mediated homology-independent targeted integration. *Nat.* 2016;540(7631):144-149. doi:10.1038/nature20565
  28. Wu J, Corbett AH, Berland KM. The Intracellular Mobility of Nuclear Import Receptors and NLS Cargoes. *Biophys J.* 2009;96(9):3840-3849. doi:10.1016/J.BPJ.2009.01.050
  29. Nishiyama J, Mikuni T, Yasuda R. Virus-Mediated Genome Editing via Homology-Directed Repair in Mitotic and Postmitotic Cells in Mammalian Brain. *Neuron.* 2017;96(4):755-768. doi:https://doi.org/10.1016/j.neuron.2017.10.004
  30. Nicoleau C, Varela C, Bonnefond C, et al. Embryonic stem cells neural differentiation qualifies the role of Wnt/ $\beta$ -Catenin signals in human telencephalic specification and regionalization. *Stem Cells.* 2013;31(9):1763-1774. doi:10.1002/STEM.1462
  31. Gribaudo S, Tixador P, Bousset L, et al. Propagation of  $\alpha$ -Synuclein Strains within Human Reconstructed Neuronal Network. *Stem Cell Reports.* 2019;12(2):230-244. doi:10.1016/J.STEMCR.2018.12.007
  32. Hottinger AF, Azzouz M, Deglon N, Aebischer P, Zurn AD. Complete and Long-Term Rescue of Lesioned Adult Motoneurons by Lentiviral-Mediated Expression of Glial Cell Line-Derived Neurotrophic Factor in the Facial Nucleus. *J Neurosci.* 2000;20(15):5587-5593. doi:https://doi.org/10.1523/jneurosci.20-15-05587.2000
  33. Duarte F, Ramosaj M, Hasanovic E, et al. Semi-automated workflows to quantify AAV

- transduction in various brain areas and predict gene editing outcome for neurological disorders. *Mol Ther - Methods Clin Dev.* 2023;29:254-270. doi:10.1016/j.omtm.2023.03.013
34. Southwell AL, Warby SC, Carroll JB, et al. A fully humanized transgenic mouse model of Huntington disease. *Hum Mol Genet.* 2013;22(1):18-34.  
doi:<https://doi.org/10.1093/hmg/dds397>
35. Brinkman EK, Chen T, Amendola M, Van Steensel B. Easy quantitative assessment of genome editing by sequence trace decomposition. *Nucleic Acids Res.* 2014;42(22):168-168.  
doi:<https://doi.org/10.1093/nar/gku936>
36. Christodoulou I, Patsali P, Stephanou C, Antoniou M, Kleanthous M, Lederer CW. Measurement of lentiviral vector titre and copy number by cross-species duplex quantitative PCR. *Gene Ther.* 2016;23(1):113-118. doi:<https://doi.org/10.1038/gt.2015.60>
37. Cambon K, Zimmer V, Martineau S, et al. Preclinical Evaluation of a Lentiviral Vector for Huntingtin Silencing. *Mol Ther - Methods Clin Dev.* 2017;5:259-276.  
doi:10.1016/J.OMTM.2017.05.001
38. Kirschneck C, Batschkus S, Proff P, Köstler J, Spanier G, Schröder A. Valid gene expression normalization by RT-qPCR in studies on hPDL fibroblasts with focus on orthodontic tooth movement and periodontitis. *Sci Reports.* 2017;7(1):1-13. doi:10.1038/s41598-017-15281-0
39. Boyle EA, Becker WR, Bai HB, Chen JS, Doudna JA, Greenleaf WJ. Quantification of Cas9 binding and cleavage across diverse guide sequences maps landscapes of target engagement. *Sci Adv.* 2021;7(8):5496.  
doi:10.1126/SCIADV.ABE5496/SUPPL\_FILE/ABE5496\_TABLES\_S1\_TO\_S19.XLSX
40. Ivanov IE, Wright A V., Cofsky JC, Palacio Aris KD, Doudna JA, Bryant Z. Cas9 interrogates DNA in discrete steps modulated by mismatches and supercoiling. *Proc Natl Acad Sci U S A.* 2020;117(11):5853-5860.  
doi:10.1073/PNAS.1913445117/SUPPL\_FILE/PNAS.1913445117.SAPP.PDF
41. Zhang L, Rube HT, Vakulskas CA, Behlke MA, Bussemaker HJ, Pufall MA. Systematic in vitro profiling of off-target affinity, cleavage and efficiency for CRISPR enzymes. *Nucleic Acids Res.* 2020;48(9):5037-5053. doi:10.1093/NAR/GKAA231
42. Bravo JPK, Liu M Sen, Hibshman GN, et al. Structural basis for mismatch surveillance by CRISPR–Cas9. *Nat.* 2022;603(7900):343-347. doi:10.1038/s41586-022-04470-1

43. Simpson BP, Yrigollen CM, Izda A, Davidson BL. Targeted long-read sequencing captures CRISPR editing and AAV integration outcomes in brain. *Mol Ther.* 2023;0(0). doi:10.1016/j.ymthe.2023.01.004
44. Nelson CE, Wu Y, Gemberling MP, et al. Long-term evaluation of AAV-CRISPR genome editing for Duchenne muscular dystrophy. *Nat Med.* 2019;25(3):427-432. doi:10.1038/s41591-019-0344-3
45. Shin JW, Shin A, Park SS, Lee JM. Haplotype-specific insertion-deletion variations for allele-specific targeting in Huntington's disease. *Mol Ther - Methods Clin Dev.* 2022;25:84-95. doi:https://doi.org/10.1016/j.omtm.2022.03.001
46. Yan S, Zheng X, Lin Y, et al. Cas9-mediated replacement of expanded CAG repeats in a pig model of Huntington's disease. *Nat Biomed Eng.* 2023:1-18. doi:10.1038/s41551-023-01007-3
47. Piao X, Meng D, Zhang X, Song Q, Lv H, Jia Y. Dual-gRNA approach with limited off-target effect corrects C9ORF72 repeat expansion in vivo. *Sci Reports.* 2022;12(1):1-15. doi:10.1038/s41598-022-07746-8
48. Gray M, Shirasaki DI, Cepeda C, et al. Full-Length Human Mutant Huntingtin with a Stable Polyglutamine Repeat Can Elicit Progressive and Selective Neuropathogenesis in BACHD Mice. *J Neurosci.* 2008;28(24):6182-6195. doi:https://doi.org/10.1523/jneurosci.0857-08.2008
49. Hodgson JG, Agopyan N, Gutekunst CA, et al. A YAC Mouse Model for Huntington's Disease with Full-Length Mutant Huntingtin, Cytoplasmic Toxicity, and Selective Striatal Neurodegeneration. *Neuron.* 1999;23(1):181-192. doi:https://doi.org/10.1016/S0896-6273(00)80764-3
50. Maeder ML, Stefanidakis M, Wilson CJ, et al. Development of a gene-editing approach to restore vision loss in Leber congenital amaurosis type 10. *Nat Med.* 2019;25(2):229-233. doi:10.1038/s41591-018-0327-9
51. Zou RS, Marin-Gonzalez A, Liu Y, et al. Massively parallel genomic perturbations with multi-target CRISPR interrogates Cas9 activity and DNA repair at endogenous sites. *Nat Cell Biol.* 2022;24(9):1433-1444. doi:10.1038/s41556-022-00975-z
52. Riesenberger S, Helmbrecht N, Kanis P, Maricic T, Pääbo S. Improved gRNA secondary structures allow editing of target sites resistant to CRISPR-Cas9 cleavage. *Nat Commun.* 2022;13(1):1-8. doi:10.1038/s41467-022-28137-7

53. Tao J, Bauer DE, Chiarle R, Assessing and advancing the safety of CRISPR-Cas tools: from DNA to RNA editing. *Nat Commun.* 2023;14:212. doi:10.1038/s41467-023-35886-6
54. Choi J, Chen W, Suiter CC, et al. Precise genomic deletions using paired prime editing. *Nat Biotechnol.* 2022;40:218-226. doi:10.1038/s41587-021-01025-z

## TABLE LEGENDS

**Table 1.** Design of sgRNA targeting the *HTT* promoter and intron 1. We selected single nucleotide polymorphisms (SNPs) located 2 kb upstream and 1.3 kb downstream of the *HTT* transcription start site with a minor allele frequency (MAF) greater than 10%, according to the 1000 genomes project phase 3. The sgHTT8P\_L and sgHTT8P\_S target the PAM-altering SNP (PAS) rs2857935 (PAM-based selectivity). The sgHTT25 (rs762855), sgHTT6 (rs28431418), sgHTT10 (rs13122415), and sgHTT2 (rs13102260) target SNPs located in target sequences of the sgRNAs (mismatch-based selectivity). The sgHTT4 targets *HTT* intron 1 and does not discriminate between wildtype and mutant alleles. Human embryonic kidney cells 293T (HEK293T) are homozygous for all selected SNPs. Neuronal progenitor cells derived from HD-patient cells (HD-NPCs) (Coriell – line GM03621) and HU97/18 mice<sup>34</sup> are heterozygous for the rs762855 and rs2857935 variants. The nucleotide variants more frequently associated to the mutant *HTT* allele are underlined.

SNP	Variant	MAF	HEK-293T genotype	HD-NPCs genotype	HU97/18 genotype	<i>HTT</i> region	sgRNA name	SNP position	sgRNA sequence (5' to 3')
rs762855	G> <u>A</u>	A=0.48	A/A	A/G	A/G	Promoter	sgHTT25	3	GACAGCAGAGAAA CAG <u>C</u> TGT
rs9996199	<u>C</u> >G	G=0.16	C/C	C/C	C/C	Promoter	---	---	-----
rs28431418	<u>I</u> >C	C=0.14	T/T	T/T	T/T	Promoter	sgHTT6	2	CAGGGCTGTCCG GGT <u>G</u> AGTA
rs2857935	<u>G</u> >C	C=0.23	G/G	C/G	C/G	Promoter	sgHTT8P_L	PAM	GCCCCGCTCCAG GCCTCGGCGG
							sgHTT8P_S	PAM	GCTCCAGGCGTC GGCGG
rs13122415	<u>C</u> >G	G=0.11	C/C	C/C	C/C	Promoter	sgHTT10	4	GGGGCTCAACGG AGAG <u>G</u> GGA
rs13102260	<u>G</u> >A	A=0.16	G/G	G/G	G/G	Promoter	sgHTT2	3	ACCCGTCCCGGC AGCC <u>C</u> CA
						Intron1	sgHTT4	No SNP	GTGGATGACATAA TGTTTT

## FIGURE LEGENDS

**Figure 1.** Design and screening of sgRNAs targeting the *HTT* promoter, exon 1, and intron 1. **(A)** Illustration of the specificity basis of sgRNAs targeting single nucleotide polymorphisms (SNPs) in the seed sequence of the sgRNA (mismatch-based selectivity) (left) or the adjacent protospacer motif (PAM-based selectivity) (right). **(B)** Schematic representation of the *HTT* promoter, exon 1, and intron 1. The sgHTT25, sgHTT6, sgHTT10, sgHTT2, and sgHTT12 are mismatch-based selective sgRNAs (blue), whereas sgHTT8P\_S and sgHTT8P\_L target a PAM-altering SNP (PAS) (brown). The sgHTT4 targets intron 1 of both the wildtype and mutant *HTT* alleles (black). The primers used for *HTT* amplification and sequencing are illustrated in the scheme and described in Table S3. **(C)** The editing efficiency of each sgRNA in HEK293T cells was quantified by TIDE four days post-transfection. Cells were transfected with two plasmids separately encoding SpCas9 and GFP under control of the PGK promoter, together with an extra plasmid encoding a sgRNA targeting the *HTT* gene. Cells transfected with only the plasmids encoding SpCas9 and GFP were used as a negative control. Because HEK293T cells are homozygous for all tested SNPs (Table 1), we generated two versions of the mismatched-based sgRNAs to facilitate the evaluation of sgRNA selectivity: one corresponding to the homologous reference sequence and the other corresponding to mismatched sgRNA. The sgHTT8P\_L and sgHTT8P\_S have no mismatched variant, as they target a PAS. The indel frequency generated by each sgRNA is presented as the mean  $\pm$  SD (N = 1, n = 3). Statistics: two-way ANOVA and multiple comparisons between matched and mismatched sgRNAs with Sidák's correction: \*\*\*\*p < 0.0001. **(D, E)** HEK293T cells were co-transduced with one LV encoding SpCas9 under the control of the PGK promoter and another LV expressing an optimized sgRNA<sup>25</sup> and mCherry under the control of the U6 and PGK promoters, respectively. Cells transduced with LVs separately encoding SpCas9 and GFP with no sgRNAs were used as a negative control. The editing efficiency of each sgRNA and their impact on *HTT* expression were analyzed at three weeks post-transduction. **(D)** The gene editing efficiency was evaluated by TIDE and **(E)** *HTT* expression by QIAcuity digital RT-PCR, with normalization against the expression of peptidylprolyl isomerase B (*PPIB*). Results are presented as the mean  $\pm$  SD (N = 1, n = 3/4). Statistics: one-way ANOVA and multiple comparisons to the control with Dunnet's correction: \*\*\*\*p < 0.0001, \*\*p < 0.01.

**Figure 2.** Deletion of *HTT* exon 1 in transduced HD-NPCs. **(A)** Schematic representation of the *HTT* exon 1 deletion in HD-NPCs. Amplification using primer set 1 (fwd1 and rev1) generates amplicons of approximately 2800 bp when the *HTT* gene is intact. Exon 1 deletion induced by HTT6/HTT4 and HTT8P/HTT4 generates shorter amplicons of 974 bp and 1053 bp, respectively. The *wtHTT* (18 CAGs) and *mHTT* (59 CAGs) alleles are heterozygous for rs2857935 (targeted by sgHTT8P\_L) and homozygous for rs28431418 (targeted by sgHTT6T) (Table 1). Thus, HTT8P/4 should exclusively excise *mHTT* exon 1, whereas HTT6/4 should delete exon 1 in both *HTT* alleles. **(B-D)** HD-NPCs were transduced with two LVs separately expressing SpCas9-BPNLS and HTT6/HTT4 or HTT8P/HTT4. Cells transduced with LVs encoding SpCas9-BPNLS and mCherry were used as a negative control. Gene editing outcomes were analyzed two weeks post-transduction. **(B)** Representative images of the agarose gels showing amplification of the *HTT* gene using primer set 1. **(C)** Semiquantitative analysis of the agarose gel images to estimate the efficiency of *HTT* exon 1 excision. Results are presented as the mean  $\pm$  SD (N = 1, n = 4). Statistics: one-way ANOVA and multiple comparisons to the control with Dunnett's correction: \*\*\*\*p < 0.0001. **(D)** TIDE analysis was performed on sequencing chromatograms from isolated full-length *wtHTT* and *mHTT* amplicons using sequencing primers hybridizing to the deleted region as shown in panel **(A)**. Results are presented as the mean  $\pm$  SD (N = 1, n = 4). Statistics: two-way ANOVA and multiple comparisons between *wtHTT* and *mHTT* with Sidák's correction.

**Figure 3.** Quantification of *HTT* gene editing outcomes in transfected HEK293T cells using digital PCR-based assays and TIDE. **(A)** Scheme illustrating the analysis of the editing outcomes generated by HTT8P/HTT4 in HEK293T cells. Cells were transfected with three plasmids separately expressing SpCas9<sup>AAV</sup>, GFP, and HTT8P/HTT4. Four days post-transfection, *HTT* exon 1 deletion was evaluated by gel agarose semiquantitative analysis or digital PCR-based promoter and intronic assays. Concerning the digital PCR assays, the amplification signals of both the promoter and intronic assays were normalized against the amplification signals of a TaqMan-based assay targeting the poly(rC)-binding protein 2 (*PCBP2*) gene.<sup>36</sup> The *PCBP2*-normalized promoter and/or intronic signals were then used to quantify the relative loss of *HTT* exon 1 relative to control samples. Additionally, indels induced by sgHTT8P\_L and sgHTT4 at the non-deleted *HTT* alleles were quantified by TIDE analysis using sequencing primers hybridizing to the deleted region. **(B)** Representative images and **(C)** semiquantitative analysis of the agarose gels after amplification of the *HTT* gene using fwd1 and rev1.

Results are presented as the mean  $\pm$  SD (N = 1, n = 4). Statistics: two-tailed unpaired t-test: \*\*\*\*p < 0.0001. **(D)** Quantification of the relative proportion of *HTT* exon 1 normalized against the number of *PCBP2* alleles in control and treated samples using the digital PCR-based promoter and intronic assays. Results are presented as the mean  $\pm$  SD (N = 1, n = 3/4). Statistics: two-way ANOVA and multiple comparisons between control and treated conditions with Sidák's correction: \*\*\*p < 0.001. **(E)** Frequency of indels at the sgRNA target sites in the full-length amplicons quantified by TIDE analysis. Results are presented as the mean  $\pm$  SD (N = 1, n = 4). Statistics: two-way ANOVA and multiple comparisons to the control with Sidák's correction: \*\*\*\*p < 0.0001. **(F)** Schematic representation of the overall *HTT* gene editing pattern and proportion of editing events measured by digital PCR and TIDE. Exon 1 was deleted in approximately 30% of all *HTT* alleles (panel **(D)**) and 20% of the full-length *HTT* alleles contained indels in at least one of the sgRNA target sites (panel **(E)**). The presence of indels in 20% of the full-length *HTT* alleles (70% of all *HTT* alleles) implies that these events occurred in 14% of all *HTT* alleles. Finally, most of the *HTT* editing events resulted in the deletion of exon 1.

**Figure 4.** Deletion of *HTT* exon 1 in HU97/18 mice by CRISPR *HTT6/HTT4*. **(A)** The striatum of HU97/18 mice was bilaterally injected with three AAV2/rh.10 vectors: one expressing SpCas9<sup>AAV</sup> (2.5 x 10<sup>9</sup> vg/hemisphere), another expressing *HTT6/HTT4* (7.5 x 10<sup>9</sup> vg/hemisphere), and the last expressing the nuclear GFP reporter (5.0 x 10<sup>8</sup> vg/hemisphere). Control mice were not injected with the AAV2/rh.10 expressing SpCas9<sup>AAV</sup>. **(B)** Illustration of the *HTT* transgenes in HU97/18 mice. The treatment is expected to induce deletions in both *mHTT* and *wtHTT* transgenes. Four weeks post-injection, 4 to 5 punches/mice were taken from the GFP-positive striatal areas for genomic DNA extraction. **(C)** Quantification of *HTT* exon 1 deletion events using the intronic digital PCR assay. Results are presented as the mean  $\pm$  SD (N = 1, n = 6 punch specimens from two control animals and n = 9 punch specimens from three treated animals). Statistics: two-tailed unpaired t-test with Welch's correction. **(D)** Frequency of indels at the sgRNA target sites in the full-length amplicons quantified by TIDE analysis. Results are presented as the mean  $\pm$  SD (N = 1, n = 4 punch specimens from two control animals and n = 9 punch specimens from three treated animals). Statistics: two-way ANOVA and multiple comparisons to the control with Sidák's correction; \*\*\*\*p < 0.0001. **(E)** Schematic representation of the overall *HTT* gene editing pattern and proportion of editing events measured by digital PCR and TIDE. Exon 1 was deleted in approximately 5% of all *HTT* alleles (panel **(C)**) and 44% of the full-length *HTT* alleles contained

indels in at least one of the sgRNA target sites (panel **(D)**). The presence of indels in 44% of the full-length *HTT* alleles (95% of all *HTT* alleles) implies that these events occurred in 42% of all *HTT* alleles. Finally, most of the *HTT* editing events resulted in the introduction of indels at the sgRNA target site(s).

**Figure 5.** Comparison of the *HTT* editing outcomes induced by HTT6/HTT4 and HTT8P/HTT4 in transfected and transduced HEK293T cells. **(A)** Two constructs separately expressing SpCas9 and HTT6/HTT4 or HTT8P/HTT4 were delivered into HEK293T cells by calcium transfection or lentiviral transduction. Cells receiving only SpCas9 and no sgRNAs were used as a negative control. Transfected and transduced cells were analyzed at 4 and 21 days after the delivery of the CRISPR components, respectively. **(B)** Schematic representation of the overall *HTT* gene editing pattern and proportion of editing events in each condition measured by digital PCR (Fig. S6A) and TIDE (Fig. S6B). While most of the *HTT* editing events in transfected HEK293T cells resulted in the deletion of exon 1, the generation of indels was the major outcome in transduced HEK293T cells.

**Figure 1**

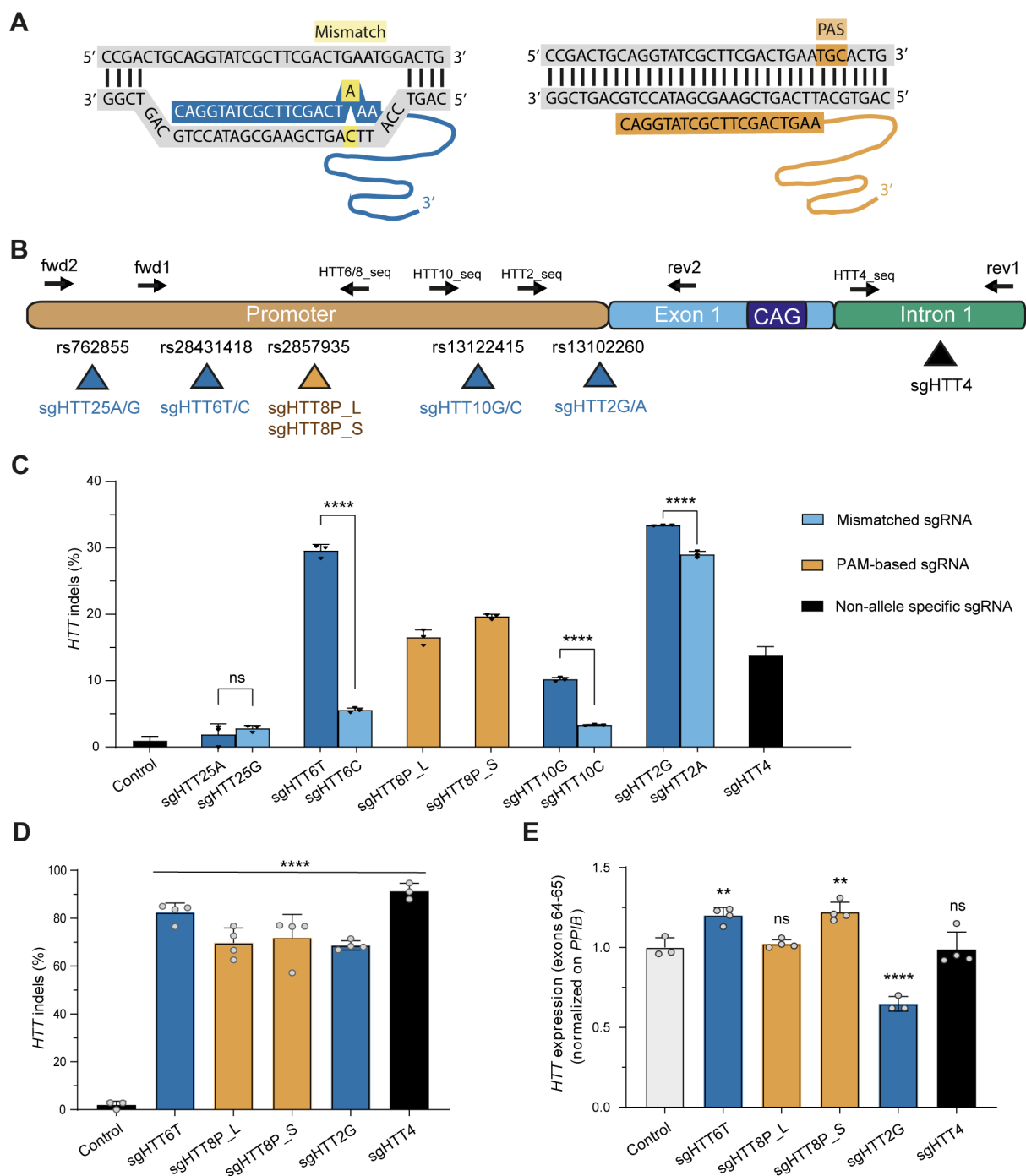


**Figure 2**

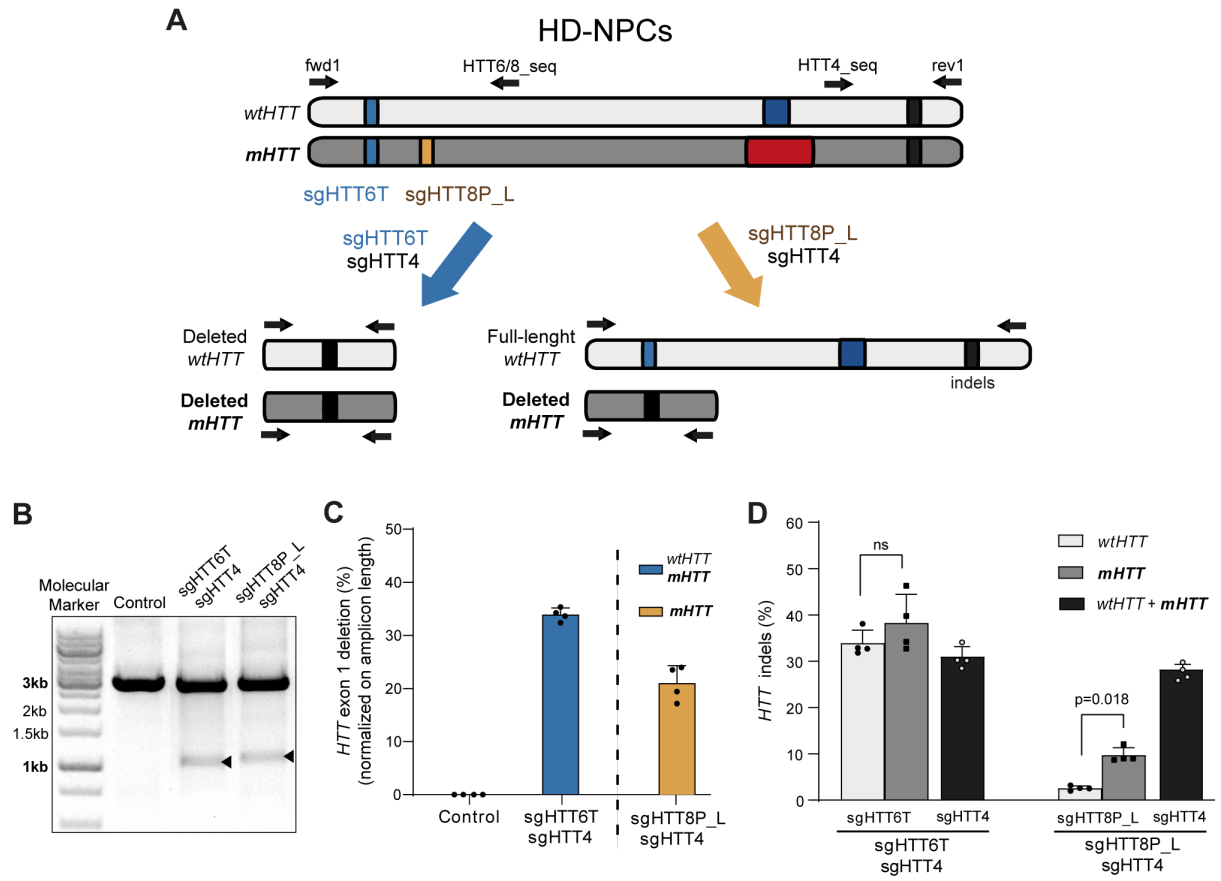


**Figure 3**

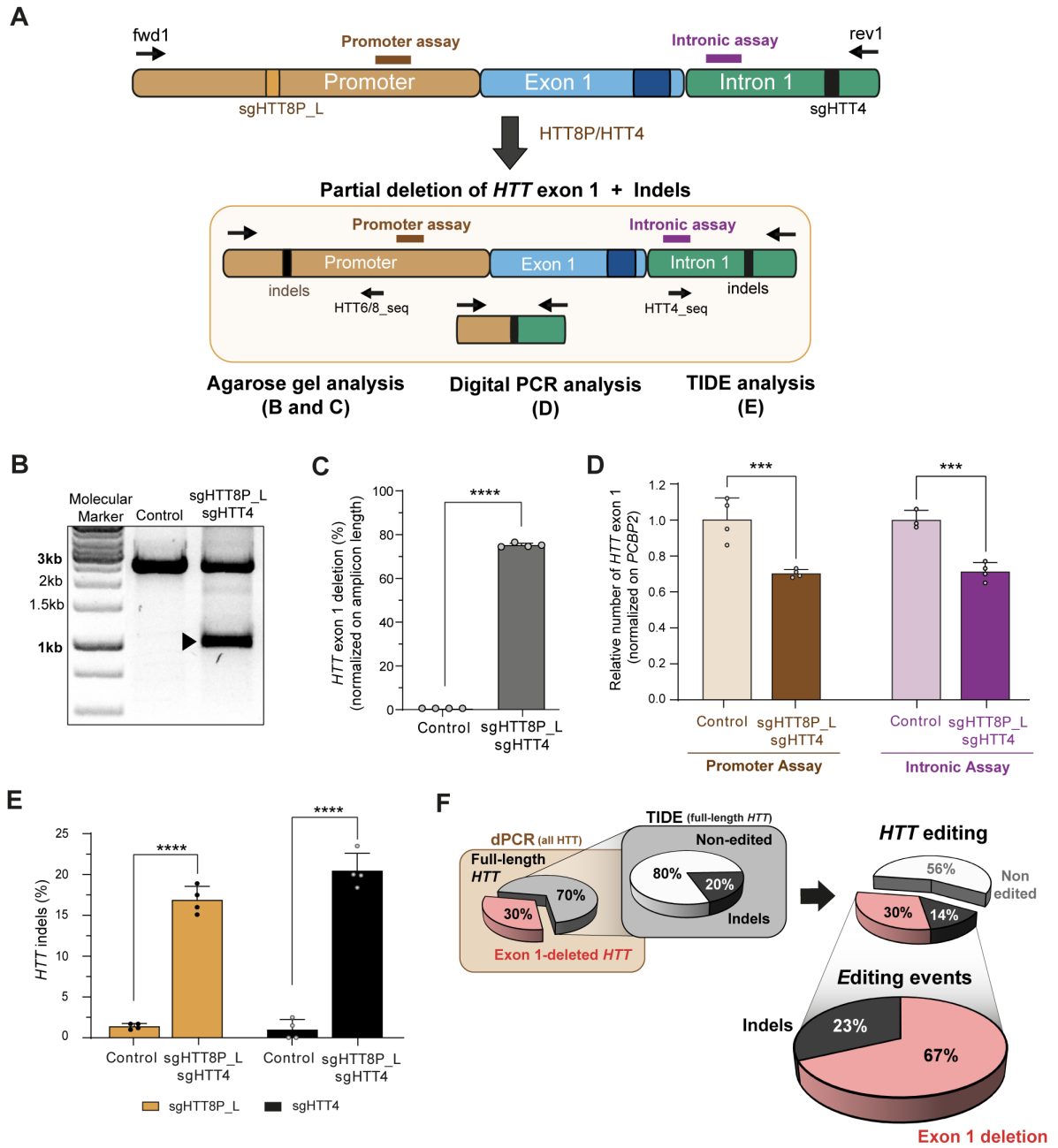


**Figure 4**

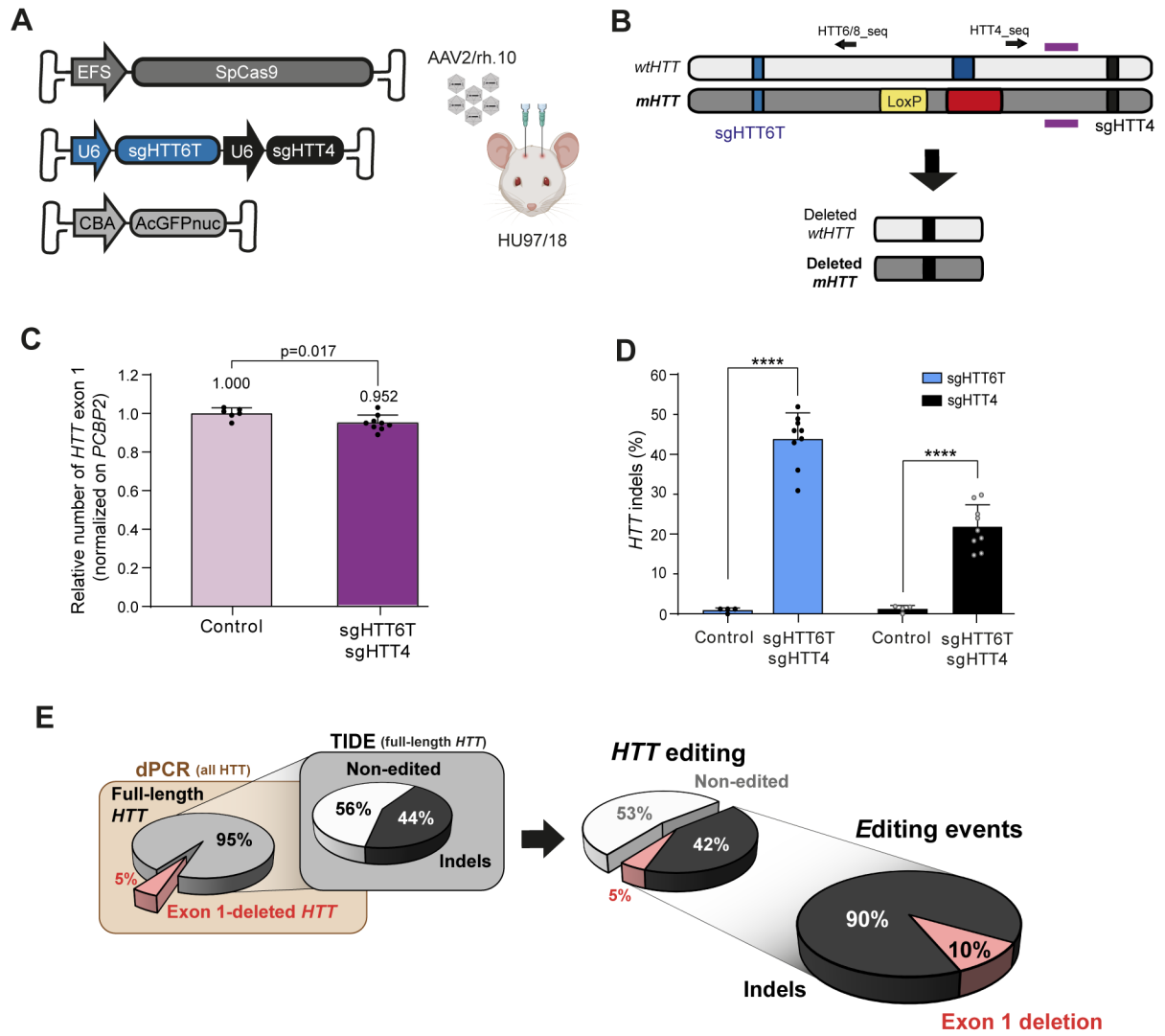
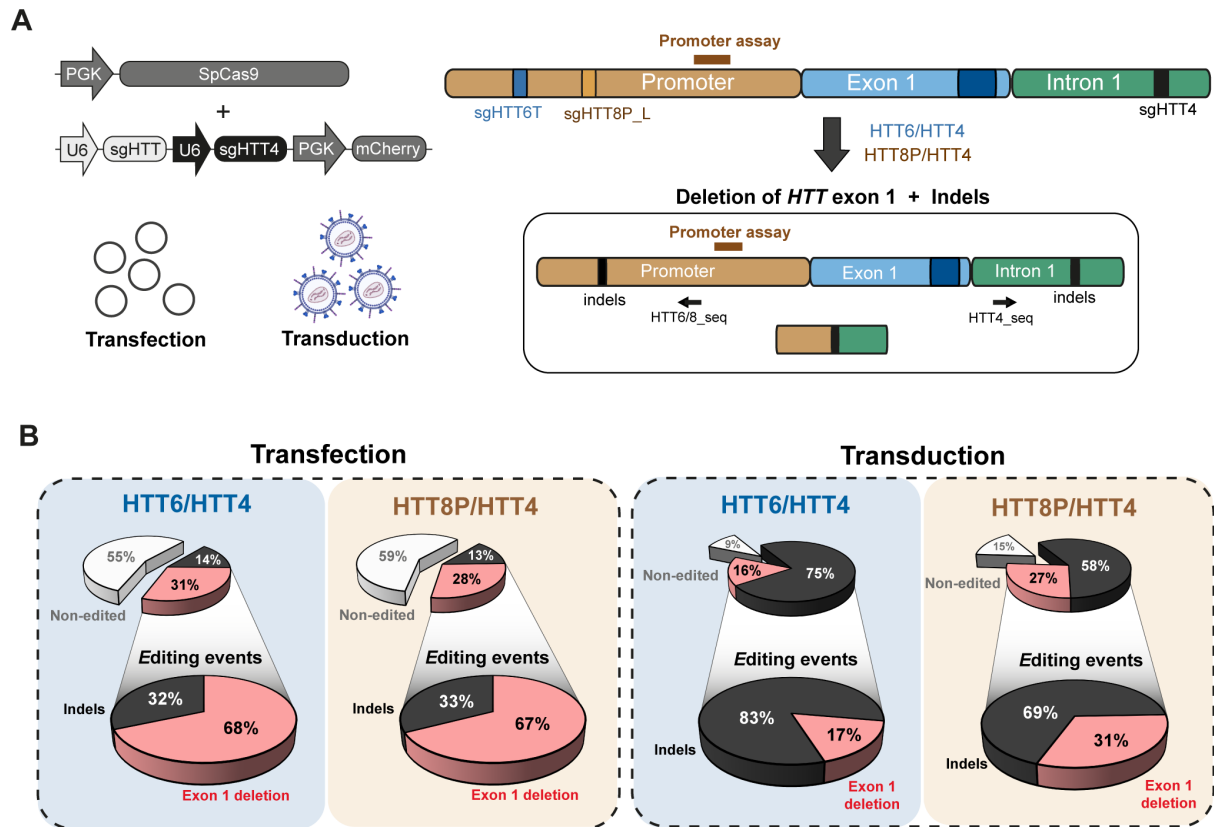
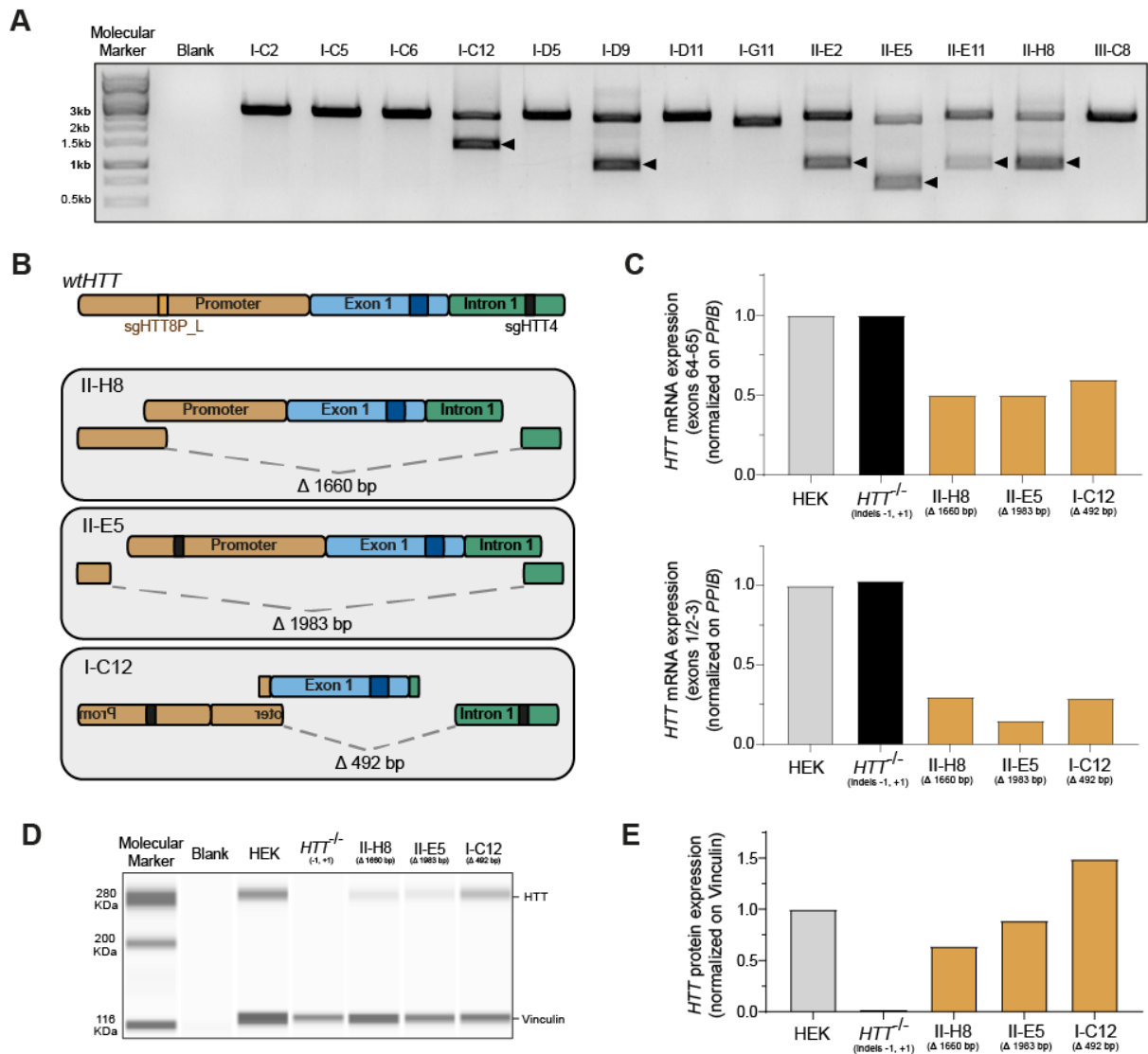


**Figure 5**



1 **SUPPLEMENTAL DATA**



2

3 **Supplemental Figure 1.** Deletion of *HTT* exon 1 in HEK293T clonal cell lines, related to Figure 2.

4 HEK293T cells were transfected with plasmids encoding SpCas9 and HTT8P/HTT4 and individual cell

5 lines subsequently cloned by dilution cloning. **(A)** Clonal lines were screened for *HTT* exon 1 deletion

6 using primer set 1. The upper fragment in the agarose gel results from the amplification of non-deleted

7 *HTT* alleles (approximately 2800 bp), whereas the lower fragments correspond to the amplification of

8 exon 1-depleted *HTT* alleles. **(B)** Illustration of the predicted rearrangements occurring in the *HTT*

9 alleles depleted of exon 1 based on Sanger sequencing. **(C)** *HTT* expression normalized against *PPIB*

10 expression levels was evaluated by RT-qPCR in non-treated HEK293T cells, a *HTT* knockout clonal

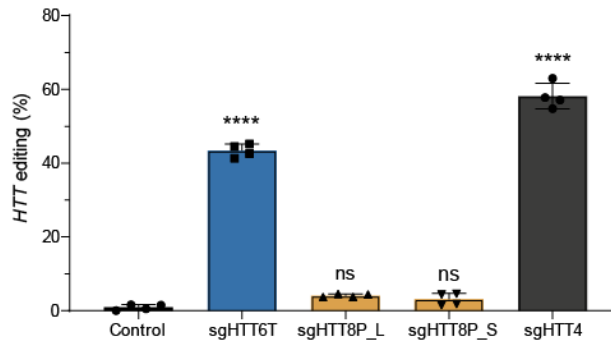
11 cell line carrying indels at the translational start site,<sup>1</sup> and in the three selected clones II-H8, II-E5, and

12 I-C12 (N = 1, n = 1). **(D)** Representative image of the capillary-based immunoassay and **(E)**

13 quantification of HTT protein levels (4C8 antibody). An antibody against vinculin was used as an internal  
14 standard for the quantitative analysis (N = 1, n = 1).

15

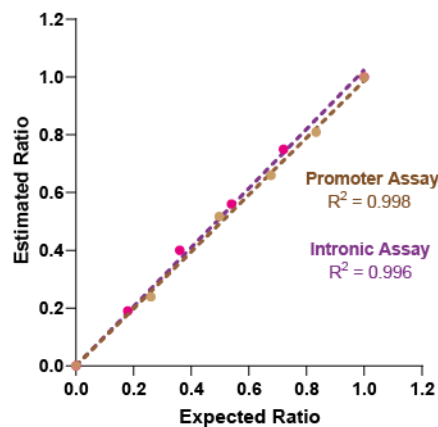
16



17

18 **Supplemental Figure 2.** Single-cut efficiency of sgHTT6T, sgHTT8P\_L, sgHTT8P\_S, and sgHTT4 in  
19 HD-NPCs, related to Figure 2. HD-NPCs were transduced with two LVs separately expressing SpCas9  
20 and sgRNA targeting the *HTT* gene (sgHTT6T, sgHTT8P\_L, sgHTT8P\_S, and sgHTT4). Cells  
21 transduced with LVs encoding SpCas9 and mCherry were used as a negative control. Gene editing  
22 outcomes were analyzed two weeks post-transduction. Results are presented as the mean  $\pm$  SD (N =  
23 1, n = 4). Statistics: one-way ANOVA and multiple comparisons to the control with Dunnet's correction:  
24 \*\*\*\*p < 0.0001.

25



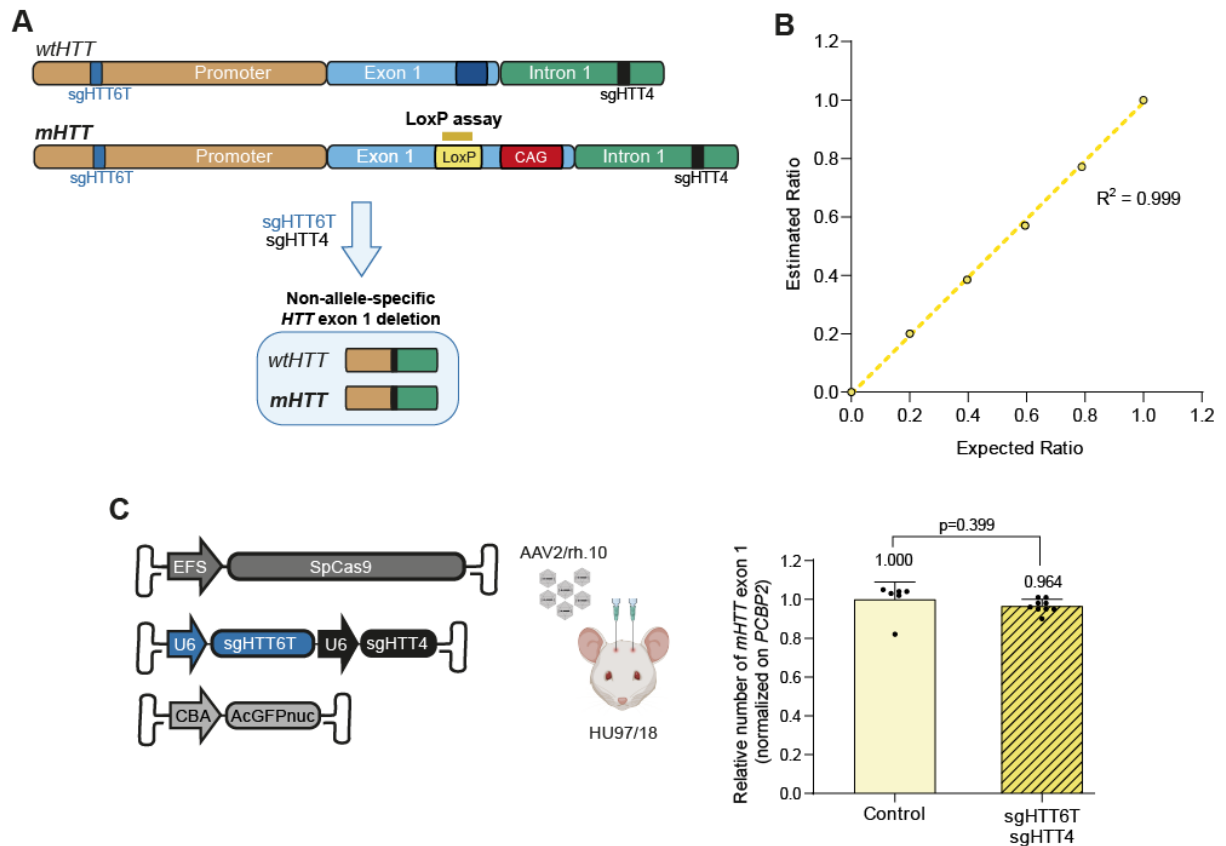
26

27 **Supplemental Figure 3.** Validation of the promoter and intronic digital PCR-based assays for  
28 quantification of *HTT* exon 1 deletion, related to Figure 3. Genomic DNA from HU97/18 (human *HTT*  
29 plus *PCBP2*)<sup>2</sup> and wildtype (*PCBP2* only) mice were mixed at increasing ratios to simulate the

30 progressive loss of *HTT* exon 1. Both assays accurately predicted the relative loss of human *HTT* exon  
 31 1 compared to the parental genomic sample from HU97/18 mice.

32

33

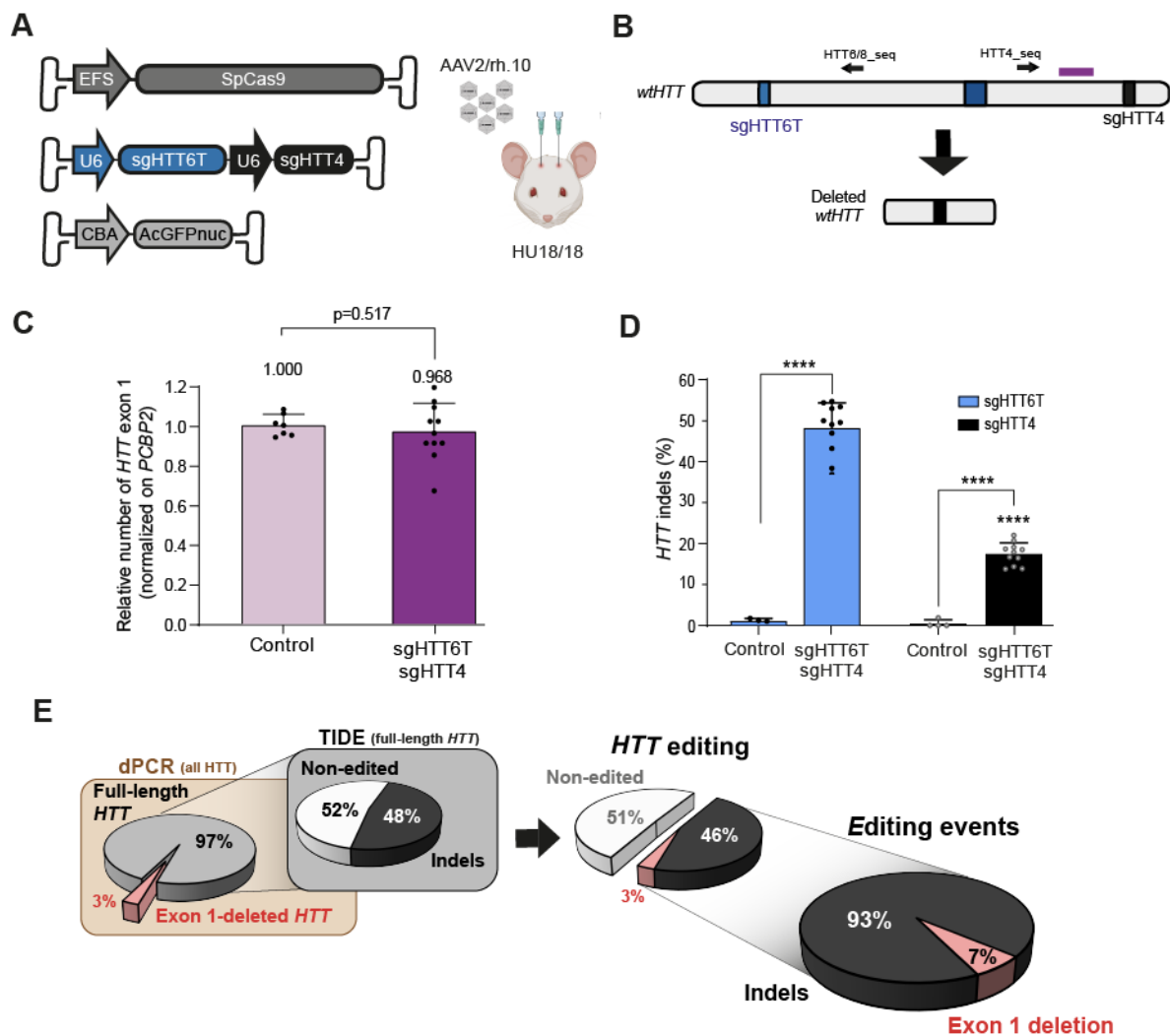


34

35 **Supplemental Figure 4.** Analysis of *mHTT* exon 1 deletion in HU97/18 by CRISPR *HTT6/HTT4* using  
 36 a mutant-specific digital PCR assay, related to Figure 4. **(A)** Illustration of the *HTT* transgenes in  
 37 HU97/18 mice. The *mHTT* transgene derived from the BACHD mice<sup>3</sup> contains 97 CAG repeats  
 38 encoding an expanded polyglutamine and a LoxP sequence at the 5'UTR. The LoxP assay is a  
 39 TaqMan-based assay specifically designed to amplify the LoxP sequence on the *mHTT* transgenes.  
 40 Amplification signals of the LoxP assay are then normalized against the amplification signals of a  
 41 TaqMan-based assay targeting the poly(rC)-binding protein 2 (*PCBP2*) gene.<sup>4</sup> The loss of *PCBP2*-  
 42 normalized LoxP signals indicates deletion of the *mHTT* exon 1. **(B)** Validation of the LoxP digital PCR-  
 43 based assay for the quantification of *mHTT* exon 1 deletion. Genomic DNA from HU97/18 (*mHTT-LoxP*  
 44 plus *PCBP2*)<sup>2</sup> and wildtype (*PCBP2* only) mice were mixed at increasing ratios to simulate the  
 45 progressive loss of the *mHTT* exon 1. **(C)** The striatum of HU97/18 mice was bilaterally injected with

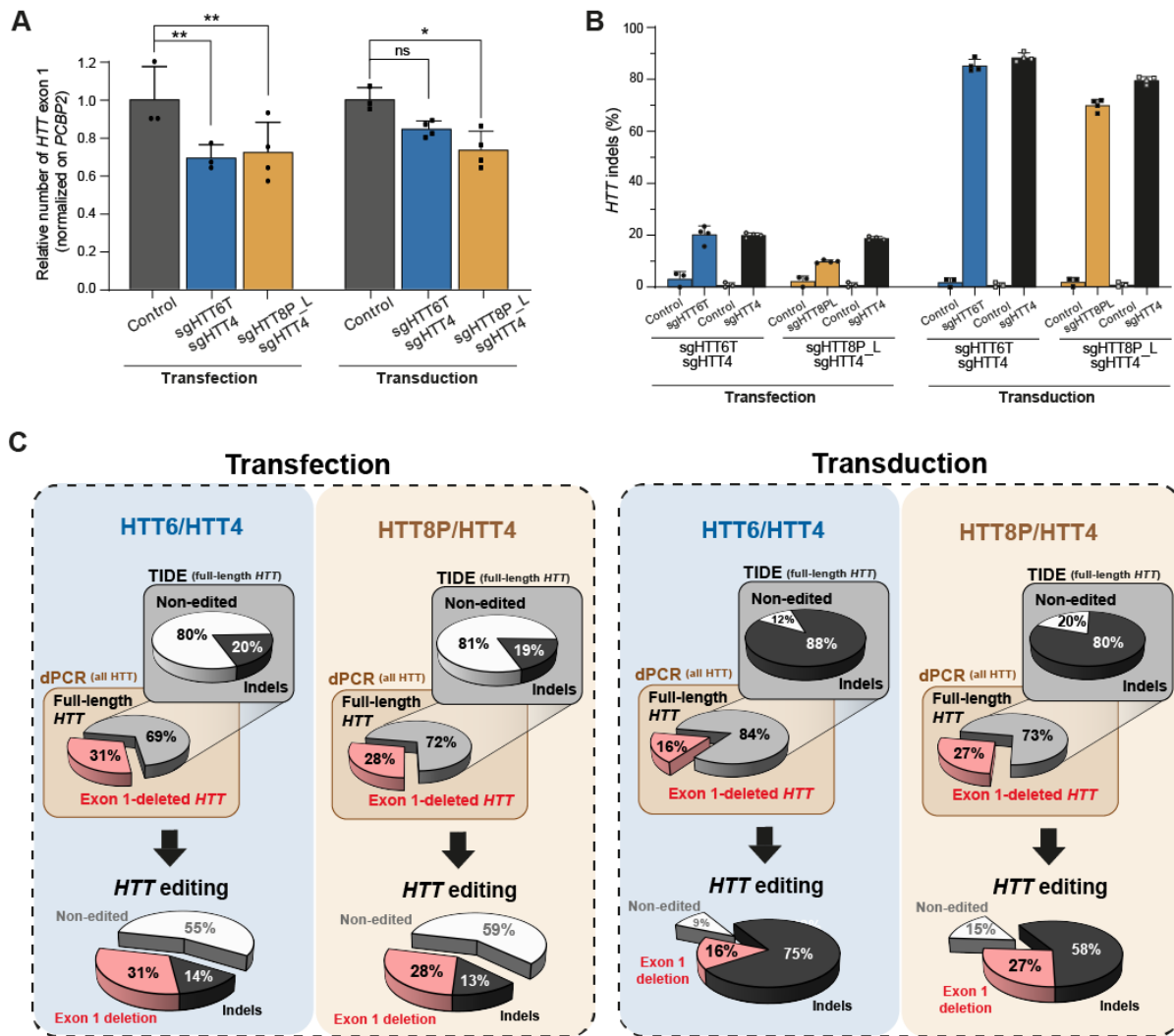
46 three AAV2/rh.10 vectors: one expressing SpCas9<sup>AAV</sup> ( $2.5 \times 10^9$  vg/hemisphere), another expressing  
 47 HTT6/HTT4 ( $7.5 \times 10^9$  vg/hemisphere), and the last expressing the nuclear GFP reporter ( $5.0 \times 10^8$   
 48 vg/hemisphere). Control mice were not injected with the AAV2/rh.10 expressing SpCas9<sup>AAV</sup>.  
 49 Quantification of *mHTT* exon 1 deletion events using the LoxP digital PCR assay. Results are presented  
 50 as the mean  $\pm$  SD (N = 1, n = 6 punch specimens from two control animals and n = 9 punch specimens  
 51 from three treated animals). Statistics: two-tailed unpaired t-tests with Welch's correction.

52  
 53



54  
 55 **Supplemental Figure 5.** Deletion of *HTT* exon 1 in HU18/18 by CRISPR HTT6/HTT4, related to Figure  
 56 4. **(A)** The striatum of HU18/18 mice was bilaterally injected with three AAV2/rh.10 vectors: one  
 57 expressing SpCas9<sup>AAV</sup> ( $2.5 \times 10^9$  vg/hemisphere), another expressing HTT6/HTT4 ( $7.5 \times 10^9$   
 58 vg/hemisphere), and the last expressing the nuclear GFP reporter ( $5.0 \times 10^8$  vg/hemisphere). Control

59 mice were not injected with the AAV2/rh.10 expressing SpCas9<sup>AAV</sup>. **(B)** Illustration of the *wtHTT*  
60 transgene in HU18/18 mice. At four weeks post-injection, 4 to 5 punches/mice were taken from the  
61 GFP-positive striatal areas for genomic DNA extraction. **(C)** Quantification of *HTT* exon 1 deletion  
62 events using the intronic digital PCR assay. Results are presented as the mean  $\pm$  SD (N = 1, n = 7  
63 punch specimens from two control animals and n = 11 punch specimens from four treated animals).  
64 Statistics: two-tailed unpaired t-tests with Welch's correction. **(D)** Frequency of indels at the sgRNA  
65 target sites in the full-length *wtHTT* amplicons quantified by TIDE analysis. Results are presented as  
66 the mean  $\pm$  SD (N = 1, n = 4 punch specimens from two control animals and n = 11 punch specimens  
67 from four treated animals). Statistics: two-way ANOVA and multiple comparisons to the control with  
68 Sidák's correction; \*\*\*\*p < 0.0001. **(E)** Schematic representation of the overall *HTT* gene editing  
69 pattern and proportion of editing events measured by digital PCR and TIDE. Exon 1 was deleted in  
70 approximately 3% of all *HTT* alleles (panel **(C)**) and 48% of the full-length *HTT* alleles contained indels  
71 in at least one of the sgRNA target sites (panel **(D)**). The presence of indels in 48% of the full-length  
72 *HTT* alleles (97% of all *HTT* alleles) implies that these events occurred in 46% of all *HTT* alleles. Finally,  
73 most of the *HTT* editing events resulted in the introduction of indels at the sgRNA target site(s).  
74



75

76

**Supplemental Figure 6.** *HTT* editing outcomes induced by HTT6/HTT4 and HTT8P/HTT4 in

77

transfected and transduced HEK293T cells, related to Figure 5. Two constructs separately expressing

78

SpCas9 and HTT6/HTT4 or HTT8P/HTT4 were delivered into HEK293T cells by calcium transfection

79

or lentiviral transduction. Cells receiving only SpCas9 and no sgRNAs were used as a negative control.

80

Transfected and transduced cells were analyzed at 4 and 21 days after delivery of the CRISPR

81

components, respectively. **(A)** Quantification of *HTT* exon 1 deletion events using the promoter digital

82

PCR assay. Results are presented as the mean  $\pm$  SD (N = 1, n = 3/4). Statistics: two-way ANOVA and

83

multiple comparisons to the control with Dunnett's correction: \*\*p < 0.01, \*p < 0.05. **(B)** Frequency of

84

indels at the sgRNA target sites in the full-length *HTT* amplicons quantified by TIDE analysis. Results

85

are presented as the mean  $\pm$  SD (N = 1, n = 3/4). Statistics: two-way ANOVA and multiple comparisons

86

between conditions with Sidák's correction: \*\*p < 0.01, \*p < 0.05. **(C)** Schematic representation of the

87

overall *HTT* gene editing pattern in each condition measured by digital PCR and TIDE.

88 **Supplemental Table 1.** List of sgRNAs ordered as gene strands and cloned into pENTR221 plasmids.

sgRNA name	Gene strand sequence
<b>sgHTT25A</b>	GTTCTGTATGAGACCACAGATCTGACAGCAGAGAAACAGCTGTGTTTTAGAGCTAGAAATAGCAA GTTAAAATAAGGCTAGTCCGTTATCAACTTGAAAAAGTGGCACCGAGTCGGTGCTTTTTTAGATCG GATCCAAGCTTCCAGGCTAGTCCGTTATCAACTTGAAAAAGTGGCACCGAGTCGGTGCTTTTTTAG ATCGGATCCAAGCTTCCA
<b>sgHTT25G (mismatch)</b>	GTTCTGTATGAGACCACAGATCTGACAGCAGAGAAACAGCCGTGTTTTAGAGCTAGAAATAGCAA GTTAAAATAAGGCTAGTCCGTTATCAACTTGAAAAAGTGGCACCGAGTCGGTGCTTTTTTAGATCG GATCCAAGCTTCCAGGCTAGTCCGTTATCAACTTGAAAAAGTGGCACCGAGTCGGTGCTTTTTTAG ATCGGATCCAAGCTTCCA
<b>sgHTT6T</b>	ACAAGATCTCAGGGCTGTCCGGGTGAGTAGTTTCAGAGCTATGCTGGAACAGCATAGCAAGTTG AAATAAGGCTAGTCCGTTATCAACTTGAAAAAGTGGCACCGAGTCGGTGCTTTTTTAGATCGGATC CAAGCTTACATAGTCCGTTATCAACTTGAAAAAGTGGCACCGAGTCGGTGCTTTTTTAGATCGGAT CCAAGCTTACA
<b>sgHTT6C (mismatch)</b>	ACAAGATCTCAGGGCTGTCCGGGTGAGCAGTTTCAGAGCTATGCTGGAACAGCATAGCAAGTTG AAATAAGGCTAGTCCGTTATCAACTTGAAAAAGTGGCACCGAGTCGGTGCTTTTTTAGATCGGATC CAAGCTTACATAGTCCGTTATCAACTTGAAAAAGTGGCACCGAGTCGGTGCTTTTTTAGATCGGAT CCAAGCTTAC
<b>sgHTT10C</b>	GTTCTGTATGAGACCACAGATCTGGGGCTCAACGGAGAGGGGAGTTTTGAGCTAGAAATAGCAAG TTAAAATAAGGCTAGTCCGTTATCAACTTGAAAAAGTGGCACCGAGTCGGTGCTTTTTTAGATCGG ATCCAAGCTCCAGGCTAGTCCGTTATCAACTTGAAAAAGTGGCACCGAGTCGGTGCTTTTTTAGAT CGGATCCAAGCTTCCA
<b>sgHTT10G (mismatch)</b>	GTTCTGTATGAGACCACAGATCTGGGGCTCAACGGAGAGCGGAGTTTTAGAGCTAGAAATAGCAA GTTAAAATAAGGCTAGTCCGTTATCAACTTGAAAAAGTGGCACCGAGTCGGTGCTTTTTTAGATCG GATCCAAGCTTCCAGGCTAGTCCGTTATCAACTTGAAAAAGTGGCACCGAGTCGGTGCTTTTTTAG ATCGGATCCAAGCTTCCA
<b>sgHTT2G</b>	GTTCTGTATGAGACCACAGATCTACCCGTCCCGGCAGCCCCAGTTTTAGAGCTAGAAATAGCAA GTTAAAATAAGGCTAGTCCGTTATCAACTTGAAAAAGTGGCACCGAGTCGGTGCTTTTTTAGATCGG ATCCAAGCTTCCAGGCTAGTCCGTTATCAACTTGAAAAAGTGGCACCGAGTCGGTGCTTTTTTAGA TCGGATCCAAGCTTCCA
<b>sgHTT2A (mismatch)</b>	GTTCTGTATGAGACCACAGATCTACTCGTCCCGGCAGCCCCAGTTTTAGAGCTAGAAATAGCAA GTTAAAATAAGGCTAGTCCGTTATCAACTTGAAAAAGTGGCACCGAGTCGGTGCTTTTTTAGATCG GATCCAAGCTTCCAGGCTAGTCCGTTATCAACTTGAAAAAGTGGCACCGAGTCGGTGCTTTTTTAG ATCGGATCCAAGCTTCCA
<b>sgHTT4</b>	GGACTATCATATGCTTACCGTAACCTGAAAGTATTTTCGATTTCTTGGGTTTATATATCTTGTGAAAA GGACGAAACACCGTGGATGACATAATGCTTTGTTTTAGAGCTAGAAATAGCAAGTTAAAATAAGGC TAGTCCGTTATCAACTTGAAAAAGTGGCACCGAGTCGGTGCTTTTTTCATAGCCATGGGCGGCCG CTCTAGACACCGTGGATGACATAATGCTTTGTTTTAGAGCTAGAAATAGCAAGTTAAAATAAGGCT AGTCCGTTATCAACTTGAAAAAGTGGCACCGAGTCGGTGCTTTTTTCATAGCCATGGGCGGCCG TCTAGA

89

90

91

92

93

94 **Supplemental Table 2.** List of sgRNAs ordered as oligonucleotides and cloned into pMK entry  
 95 plasmids. The generated overhangs after oligonucleotide annealing are underlined. In certain sgRNAs,  
 96 an extra guanine was added at the 5' end to facilitate U6-driven expression. The enzymes used for  
 97 cloning of the annealed oligos and the position of the cassette in the universal pMK entry plasmid are  
 98 indicated in the second column.

sgRNA name	Enzyme # cassette	Forward oligo (5' – 3')	Reverse oligo (5' – 3')
sgHTT6T	Bsal #1	<u>CACCGC</u> CAGGGCTGTCCGGTGAGTA	<u>AAACTACTC</u> ACCCGGACAGCCCTGC
sgHTT6C (mismatch)	Bsal #1	<u>CACCGC</u> CAGGGCTGTCCGGTGAGCA	<u>AAACTGCTC</u> ACCCGGACAGCCCTGC
sgHTT8P_L	Bsal #1	<u>CACCGCCCCG</u> CTCCAGGCGTCGGCGG	<u>AAACCCGCCG</u> CACGCTGGAGCGGGGC
sgHTT8P_S	Bsal #1	<u>CACCGCTCC</u> AGGCGTCGGCGG	<u>AAACCCGCCG</u> CACGCTGGAGC
sgHTT2G	Bsal #1	<u>CACCGTGGGGG</u> CTGCCGGGACGGGT	<u>AAACACCCGT</u> CCCGGCAGCCCCAC
sgHTT4	SapI #2	<u>ACCGTGGATG</u> ACATAATGCTTTT	<u>AACA</u> AAAAGCATTATGTCATCCAC

99

100

101 **Supplemental Table 3.** List of primers used for Sanger sequencing and respective targeted  
 102 sequencing sites.

sgRNA target site	Amplification primer set	Sequencing primer	Primer sequence (5' – 3')
sgHTT25	Set 2 (fwd2/rev2)	HTT25_seq / fwd2	TCGAACTCCTGACCTCTGGT
sgHTT6 sgHTT8P_L sgHTT8P_S	Set 1 (fwd1/rev1)	HTT6/8_seq	GACTGCATGGTAAGGGAGGC
sgHTT10	Set 1 (fwd1/rev1)	HTT10_seq	GCCCCACGGCGCCTTGCGTCC
sgHTT2	Set 1 (fwd1/rev1)	HTT2_seq	TGCTGCTGGAAGGACTTGAG
sgHTT1	Set 1 (fwd1/rev1)	HTT1_seq	GCCTGTCTGAATTCACCGA
sgHTT4	Set 1 (fwd1/rev1)	HTT4_seq	TTGCTGTGTGAGGCAGAACCTGCGG

103

104

105

106 **REFERENCES**

- 107 1. Duarte F, Ramosaj M, Hasanovic E, et al. Semi-automated workflows to quantify AAV  
108 transduction in various brain areas and predict gene editing outcome for neurological  
109 disorders. *Mol Ther - Methods Clin Dev.* 2023;29:254-270. doi:10.1016/j.omtm.2023.03.013
- 110 2. Southwell AL, Warby SC, Carroll JB, et al. A fully humanized transgenic mouse model of  
111 Huntington disease. *Hum Mol Genet.* 2013;22(1):18-34.  
112 doi:<https://doi.org/10.1093/hmg/dds397>
- 113 3. Gray M, Shirasaki DI, Cepeda C, et al. Full-Length Human Mutant Huntingtin with a Stable  
114 Polyglutamine Repeat Can Elicit Progressive and Selective Neuropathogenesis in BACHD  
115 Mice. *J Neurosci.* 2008;28(24):6182-6195. doi:<https://doi.org/10.1523/jneurosci.0857-08.2008>
- 116 4. Christodoulou I, Patsali P, Stephanou C, Antoniou M, Kleanthous M, Lederer CW.  
117 Measurement of lentiviral vector titre and copy number by cross-species duplex quantitative  
118 PCR. *Gene Ther.* 2016;23(1):113-118. doi:<https://doi.org/10.1038/gt.2015.60>
- 119